INVESTIGATION OF FUNCTIONAL BRAIN CONNECTIVITY PATTERNS IN TEMPORAL LOBE EPILEPSY

by

Seda Nilgün Dumlu

B.S., in Computer Engineering, Bilkent University, 2009

M.Sc., in Medical Informatics, Middle East Technical University, 2012

Submitted to the Institute of Biomedical Engineering

in partial fulfillment of the requirements

for the degree of

Doctor

of

Philosophy

Boğaziçi University

2021

INVESTIGATION OF FUNCTIONAL BRAIN CONNECTIVITY PATTERNS IN TEMPORAL LOBE EPILEPSY

APPROVED BY:

Prof. Dr. Ahmet Ademoğlu .....
(Thesis Advisor)

Assoc. Prof. Dr. Adil Deniz Duru .....

Prof. Dr. Burak Güçlü .....

Prof. Dr. Ata Akın .....

Assoc. Prof. Dr. Esin Öztürk Işık .....

DATE OF APPROVAL: 30 April 2021

ACKNOWLEDGMENTS

I would like to express my very great appreciation to my advisor Prof. Dr. Ahmet Ademoğlu for his valuable guidance, patience and great support from the beginning till the end of my Ph.D. work. I would like to express my deep gratitude to Prof. Dr. Hesheng Liu for his precious guidance during my time at Massachusetts General Hospital and Harvard Medical School. I am grateful to Prof. Dr. Wei Sun for her valuable support in providing the data and supervision during this Ph.D. work. I also would like to express my sincere appreciation to Assoc. Prof. Dr. Adil Deniz Duru and Prof. Dr. Burak Güçlü for their constructive suggestions and help during this research.

I would like to thank my dearest friend Ayşe Sena Sarp for her endless support and standing by my side. I would like to specially thank to Kangcheng Wang, Yuxiang Yan, Fransizka Galie, Jianxun Ren, Meiling Li, Güneş Kayacı Sevinç for their valuable help and support during my time at Harvard. I also send my special thanks to Dilek Göksel Duru, Fatma Şimşek, Elif Kubat Öktem, Hüden Neşe, Moataz Assem, Esin Karahan, Ali Demir, Bige Vardar, Pınar Adanalı for their endless support and valuable friendship. I would like to thank my dearest friends Gülden Olgun and Püren Güler for always standing by my side and supporting me.

I send my sincere appreciation to my family, my academic endevaour, my father Prof. Dr. Şükrü Dumlu, my mother Nüket Dumlu and my brother, Reha Dumlu for their endless support from the beginning of my life until now. I dedicated this thesis to my unique family, without their support this work wouldn't have been possible.

This thesis study was supported by the fellowship from TÜBİTAK 2214/A International Doctoral Research Fellowship Programme.

ACADEMIC ETHICS AND INTEGRITY STATEMENT

I, Seda Nilgün Dumlu, hereby certify that I am aware of the Academic Ethics and Integrity Policy issued by the Council of Higher Education (YÖK) and I fully acknowledge all the consequences due to its violation by plagiarism or any other way.

Name :

Signature:

Date:

ABSTRACT

INVESTIGATION OF FUNCTIONAL BRAIN CONNECTIVITY PATTERNS IN TEMPORAL LOBE EPILEPSY

In this study, functional connectivity using both Pearson and partial correlation coefficients and inter-subject variability were investigated in resting state functional resonance imaging (rs-fMRI) scans that belong to healthy and temporal lobe epileptic (TLE) patient populations. The main purpose of this thesis is to reveal the discrepancies between the healthy population and the patients with TLE in terms of functional connectivity revealing the temporal dependency among different brain regions. According to inter-subject variability results, TLE population exhibited higher inter-subject variability in frontoparietal control, default mode, dorsal/ventral attention, visual, limbic and somatomotor networks in line with the broad seizure onset and propagation pathway. We mostly found a significantly reduced functional connectivity in bilateral frontoparietal control, somatomotor, default mode and ventral attention networks with an implication of dysfunctioning in attention, long/short term memory, cognitive functioning and consciousness in patients with TLE as a result of 17-network parcellation. We also found a decreased functional connectivity between/within the networks of the frontoparietal control, the default mode and the ventral attention implying that these three networks as well show a variability, although to a lesser extent. This result signifies these networks are severely deteriorated in patients with TLE. On the other hand, to compute the direct functional connectivity among different brain regions, partial correlation coefficients estimation is used. In doing so, we took advantage of Random Matrix Theory to well approximate the partial correlations, by virtue of, the inverse covariance matrices. As a result, the bilateral homologous structures in dorsal/ventral attention, frontoparietal control and default mode networks were also decreased in patient population confirming our results using Pearson's corelation coefficients.

Keywords: Resting State fMRI, Functional Connectivity, Temporal Lobe Epilepsy.

ÖZET

TEMPORAL LOB EPİLEPSİ HASTALARINDA FONKSİYONEL BEYİN BAĞLANTISALLIK ÖRÜNTÜLERİNİN İNCELENMESİ

Bu çalışmada sağlıklı bireylerin ve temporal lob epilepsi hastalarının dinlenim durumu beyin ağları arasındaki fonksiyonel bağlantısallık Pearson, kısmi ilinti katsayıları ve kişiler arası değişkenlik ölçülmüştür. Bu tezin temel amacı temporal lob epilepsi hastalarının beyin ağlarındaki fonksiyonel bağlantısallığın sağlıklı bireylerden farklılığını ortaya koymaktır. Kişiler arası değişkenlik sonuçlarına göre, temporal lob epilepsi hastaları çeşitli nöbet başlangıç odağına ve yayılımına uyumlu olarak sağlıklı bireylere oranla frontopariyetal kontrol, olağan durum, dorsal/ventral dikkat, görsel, limbik ve somatomotor ağlarda daha fazla fonksiyonel bağlantısallık çeşitliliği göstermiştir. 17-ağ bölütlemesi fonksiyonel bağlantısallık sonuçlarına göre temporal lob hastalarında çoğunlukla iki taraflı olarak frontopariyetal kontrol, olağan durum, ventral dikkat ve somatomotor ağlarında dikkat, kısa-uzun süreli hafıza, biliş ve bilinç fonksiyon bozukluğu ile uyumlu olarak istatistiksel olarak anlamlı bir fonksiyonel bağlantısallık düşüklüğü saptanmıştır. Fonksiyonel bağlantısallığın çoğunlukla azaldığı ve kişiler arası değişkenlik farkının görece azaldığı ağlar frontopariyetal kontrol, olağan durum, ventral dikkat ağları olmuştur. Bu sonuç, bu üç ağın temporal lob epilepsi hastalarında oluşmuş fonksiyonel bağlantı bozukluğuna işaret etmektedir. Diğer yandan farklı beyin bölgeleri arasındaki doğrudan fonksiyonel ilişkiyi bulmak için kısmi korelasyon katsayısı hesaplanmaktadır. Bunun için "Rastgele Matris Teorisi" kullanılarak kovaryans matrisin tersi, dolayısıyla kısmi korelasyon katsayıları hesaplanmıştır. Bunun sonucunda hasta populasyonunda dorsal/ventral dikkat, frontopariyetal kontrol ve olağan durum ağlarına ait iki taraflı beyin bölgelerinde fonksiyonel bağlantısallığın azaldığı tespit edilmiş olup, bu bulgular Pearson korelasyon katsayısı ile elde ettiğimiz sonuçları doğrulamaktadır.

Anahtar Sözcükler: Temporal Lob Epilepsi, Fonksiyonel Bağlantısallık, Dinlenim Durumu Fonksiyonel Manyetik Rezonans Görüntüleme.

TABLE OF CONTENTS

LIST OF FIGURES

LIST OF TABLES

LIST OF SYMBOLS

O_2	Oxygen
Hz	Hertz
r	The Pearson's correlation
E	Expected value
S	Sample covariance
p_1	Number of appended region of interests to the end of matrix
p	Number of region of interests
p_0	Number of region of interests in each sub-matrix
R^2	Coefficient of determination
AR^2	Average coefficient of determination
SS	Sum of squares
λ	Lamda
X_{obs}	The actual values observed for the model
X_{model}	Values predicted by the model
Y_{obs}	The actual values observed for the model
Y_{model}	Values predicted by the model

LIST OF ABBREVIATIONS

DMN	Default Mode Network
fMRI	functional Magnetic Resonance Imaging
EEG	Electroencephalography
SOZ	Seizure Onset Zone
EZ	Epileptogenic Zone
MRI	Magnetic Resonance Imaging
PET	Positron Emission Tomography
DTI	Diffusion Tensor Imaging
iEEG	Invasive(Intracranial) Encephalography
icEEG	intracortical Encephalography
ICA	Independent Component Analysis
GLM	General Linear Model
PCA	Principal Component Analysis
ROI	Region of Interest
RSNs	Resting State Networks
TLE	Temporal Lobe Epilepsy
rs-fMRI	Resting State Functional Magnetic Resonance Imaging
SUDEP	Sudden Unexplained Death in Epilepsy
AEDs	Antiepileptic Drugs
AR	Autoregressive Model
E-RSMFC	Extended Random Subspace Method For Functional Connectivity
FDR	False Discovery Rate
MSE	Mean Squared Error
NMSE	Normalized Mean Squared Error

1. INTRODUCTION

Human brain consists of a large number of anatomical regions which are unique to each individual. This brings the notion of quantifying the variability in each individual brain. Hence, investigating the individual differences and the brain network alterations in neurodegenerative diseases have been an important and challenging research area in the field of neuroscience. According to a classical theory, the function of human brain has two different aspects, i.e., functional segregation and functional integration. Functional segregation states that each brain region is specialized according to its function, whereas functional integration emphasizes how different brain regions functionally correlate with each other [1],[2]. To understand the latter, neuroscientific studies explore the functional integration of the human brain via effective and functional connectivity [3]. Moreover, the network activity of the brain is assessed by three different connectivity measures. First of all, the structural connectivity explains the white matter tracts, the so-called physical connections between brain regions. Secondly, the correlation of the activities in different brain regions is defined by the functional connectivity. Functional connectivity has been used in intrinsic functional connectivity and task-based functional connectivity. Specifically, task based functional connectivity can be assessed under two different conditions, when subject performs i) a specific task (visual network while observing pictures) ii) response to the external stimuli. Intrinsic functional connectivity refers to internal task-free activity of the brain during resting state [4]. Lastly, the effective connectivity measures the cause and effect relation between different regions of the brain (Figure 1.1 and Figure 1.2) [2],[5],[6].

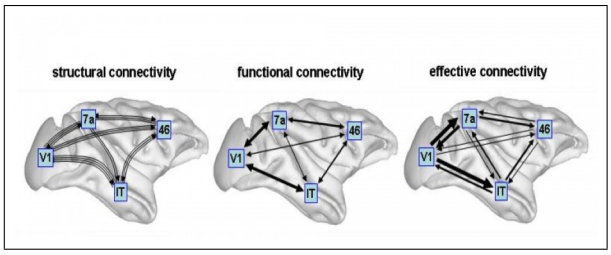

Figure 1.1 Types of Brain Connectivity (Adapted from [7]).

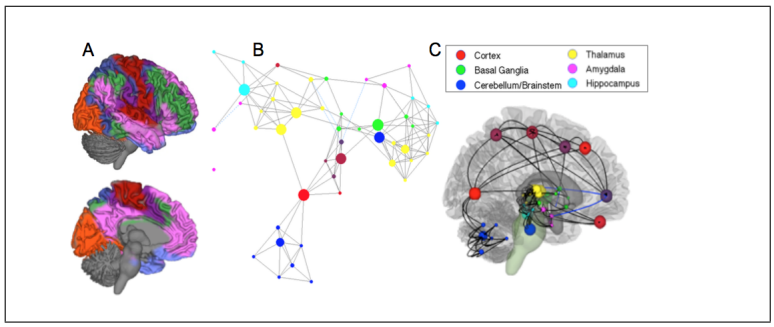

Figure 1.2 (A) Functional connectivity of the brain. (B) Co-activations from a meta-analysis of 148 neuroimaging studies. The nodes (circles) denote regions or networks for the corresponding anatomical regions, The edges (lines) represent simultaneous activation between pairs of regions or networks, The size of each circle denotes the connection strength between networks. C) Representation of the connections in the anatomical space of the brain (Adapted from [8]).

Functional magnetic resonance imaging (fMRI) is an indirect measure of blood oxygenated level dependent(BOLD) response [9]. fMRI mainly measures the indirect BOLD contrast whose mechanism relies on the increase in blood flow and oxygenation due to neuronal activity. Due to its high spatial resolution, the activation over the brain regions can be precisely observed in fMRI which contain large number of voxels defined as cubes with equal size [8],[10]. fMRI data is collected under two main procedures that are task based and resting state. In the case of task based fMRI, subjects are instructed to perform a certain task, whereas for resting state fMRI they are informed not to perform any task during scanning process. For task based fMRI, there is stimulus locked time series data, whereas for resting state fMRI, there is spontaneous, low frequency fluctuations ($<$0.1 Hz) [11],[12]. A sample fMRI and its timing sequences are depicted in Figure 1.3.

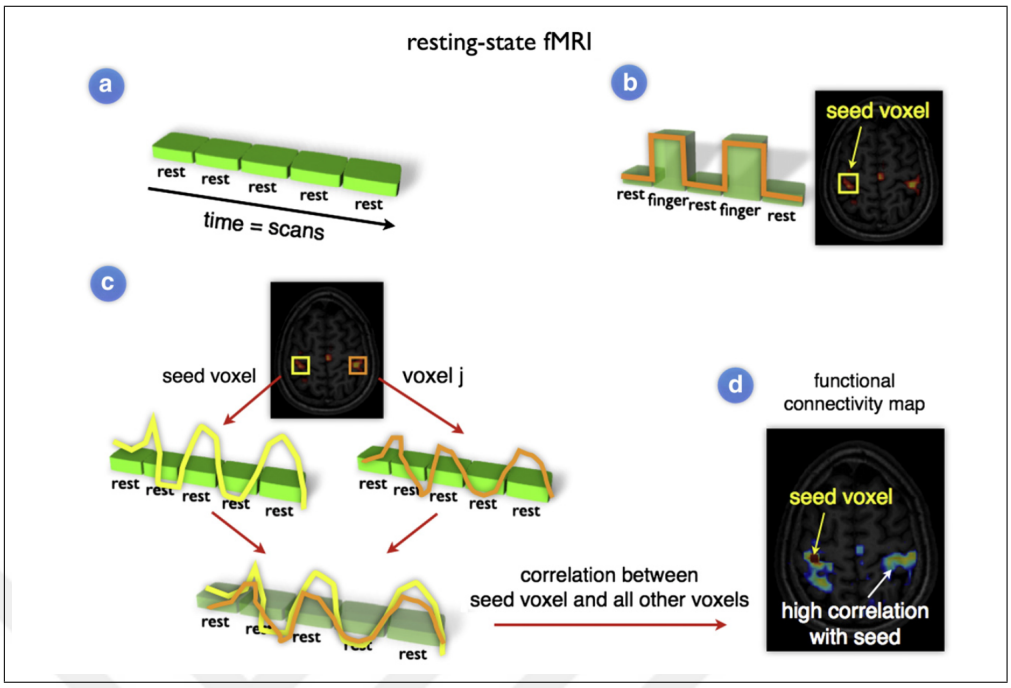

Figure 1.3 (a) Experimental design for resting state fMRI (b) Experimental design for task based fMRI, subjects are instructed to perform right hand finger tapping (c) To assess functional connectivity in resting state, the seed voxel or region (ROI) in left precentral gyrus area is chosen, and it is highly correlated with voxel j (d) Whole brain functional connectivity map according to seed voxel (voxels that are highly correlated with seed is shown) (Adapted from [13]).

Numerous article have been published recently that try to understand how the brain activity changes under different physiological and pathological conditions [14],[15]. Although source localization is critical, with the new advances in the field of computational neuroscience, connectivity studies take a step forward with their ability to find the relations among different regions of the brain. In this regard, investigation of intrinsic activity in resting state networks requires an examination of functional connectivity which gives an insight about the ongoing brain activity [16],[17],[18]. As an important contribution, functional connectivity maps illustrate the origins of pathologic brain activity in neurodegenerative diseases. Within this context, epilepsy is one of the common diseases among others such as Alzheimer's, schizophrenia, stroke and amyotrophic lateral sclerosis. Every one out of 26 people may suffer from an epileptic

seizure in his or her lifespan [19]. It is a chronic disease which is caused by the excessive neuronal activity [20]. Thus, it may result motor, cognitive and sensory impairments [21]. The disruption not only results in a deterioration in functional networks but it also causes a high variability in their functional networks in patients with TLE [22],[23],[24]. The correlation coefficient is one of the most commonly used measures that assesses the functional connectivity. However, brain regions can be connected in several different forms. In other words, they may have a direct relation or may have a connection via a common driving source or may have been interconnected to each other through the interference of multiple brain regions [25]. Since correlation coefficient yields marginal dependency between regions [26], partial correlation coefficient has been used to compute the direct relation between regions by regressing out the interference of other regions [26],[27].

The purpose of this study is to investigate the functional connectivity disturbances and inter-subject variability of patients with TLE by using their rs-fMRI scans with both correlation and partial correlation coefficients. According to our hypothesis, the patient group shows more variability in frontoparietal control, default mode, somatomotor, visual, limbic and attention networks compared to healthy controls which may also relate to their hypo- or hyper-functional connectivity patterns based on a widespread cognitive deficit.

In the following, the literarature review is presented in Chapter 2, the functional connectivity methodology is given in Chapter 3. In Chapter 4, the findings related to functional connectivity in patients with epilepsy and healthy group is presented. Finally, the interpretations of the functional connectivity and variability patterns in epileptic patients as well as in healthy subjects and their future prospects are explained in Chapter 5.

2. BACKGROUND AND LITERATURE REVIEW

2.1 Synthesis of the Literature Review

2.1.1 Concept of fMRI

fMRI is a widely used non-invasive technique that does not expose the participants to any known ionizing radiation [28]. From the physiological perspective, fMRI measures the indirect BOLD response which is based on the blood flow and oxygenation. This mechanism relies on hemoglobin and deoxyhemoglobin changes in the blood flow. Therefore, hemoglobin is a protein which transmits oxygen (O_2) molecules to the cells. The oxygenated blood carries oxyhemoglobin which is formed when O_2 binds to protein, and if it releases one of its O_2, the protein is called as deoxyhemoglobin. By the increase of synaptic activity in the related region of the brain, there is also an ATP need that arises from fulfilling this activity. By virtue of this demand, the blood flow suddenly increases which leads to high rate of O_2 transmission. When O_2 increases in the blood, the deoxyhemoglobin decreases and oxyhemoglobin increases suddenly. This signal is defined as blood oxygenated level dependent (BOLD) response. Since deoxyhemoglobin is paramagnetic, MRI signal increases with an 2-4% amount due to the reduction of deoxyhemoglobin [29],[30]. As a result, fMRI utilizes this signal increase to reveal the activity related brain regions [8]. Sample fMRI time series can be observed in Figure 2.1.

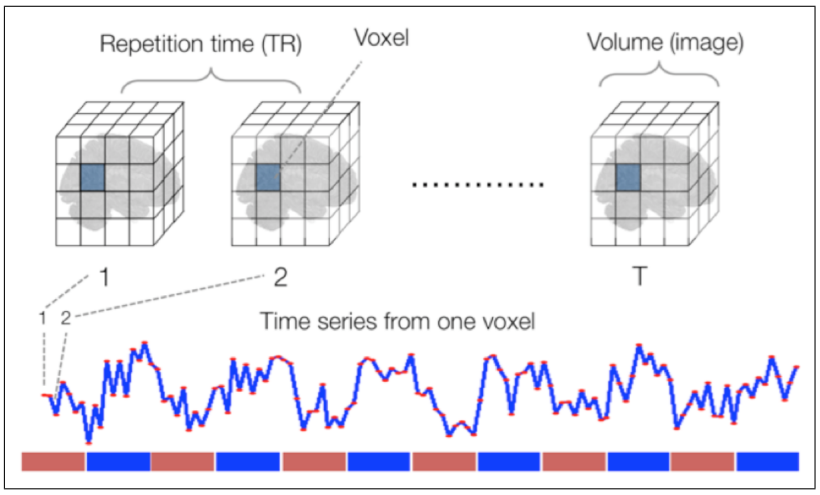

Figure 2.1 fMRI time series (Adapted from [8]).

2.1.2 Resting State Functional Connectivity in Healthy Subjects and Epileptic Patients through fMRI

Resting state fMRI (Rs-fMRI) reveals the spontaneous low frequency (<0.1 Hz) fluctuations in the BOLD signal due to neuronal intrinsic activity [13]. The motivation behind studying resting state fMRI is, to deeply understand the brain energy metabolism, during the spontaneous neural activity [11]. The first resting state fMRI was conducted by [31]. In this study, for the first experiment, subjects were instructed not to do any task including motor, cognitive, attention or language. As a second experiment, subjects were instructed to perform a bilateral finger tapping task which activates the left somatosensory cortex chosen as a seed region. As a result, they showed the left and right primary motor cortices are highly correlated with each other during resting state as well as finger tapping task (Figure 1.3). The results suggest that functionally correlated regions during task based paradigms also correlate during resting state. To conclude, we can predict task based functional brain maps by interpreting the neuronal spontaneous activity [11],[31]. On the other hand, there has been a debate on the reliability of the resting state fMRI, as there are also other low frequency signals due to cardiac and respiratory oscillations, which make one to think that there might be a functional correlation between different brain regions arising from such signals.

There are resting state networks, highly correlated in terms of spontaneous activity with each other, which are located in totally different brain regions as well as sharing the same function (as in the case of motor, auditory and visual networks) anatomical regions [13]. In addition to this, the cardiac (0.6-1.2 Hz) and the respiratory (0.1-0.5 Hz) oscillations typically show different frequency fluctuations than ongoing spontaneous activity [32]. Furthermore, spontaneous BOLD fluctuations are also correlated with the amplitudes of high frequency electrical activity of the brain, such as gamma frequency band whose range is between 60-100 Hz [11]. Additionally, the theory behind resting state fMRI is explained in [17], (p.833) "the functional regions active during rest parallel those regions active during tasks that require subjects to engage in internally directed mental operations". The relation between RSNs and EEG rhythms are illustrated in [33] which indicates that BOLD DMN activity has a positive significant correlation with alpha and beta rhythms of EEG (Figure 2.2). According to their results, each network has more than one rhythm implying that although the neuronal oscillation frequencies are different, these neurons are within the same functional system.

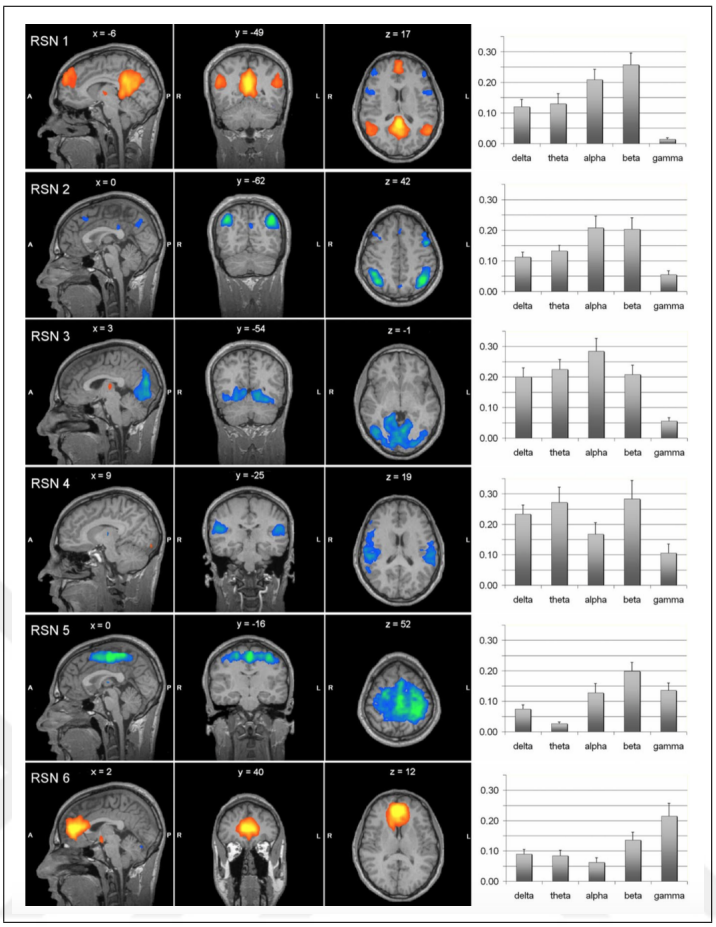

Figure 2.2 Resting state networks using EEG and fMRI. (Left) Sagittal, coronal, and axial spatial maps for DMN (IC1), dorsal attention network (IC2), visual processing (IC3), auditory-phonological system (IC4), sensorimotor network (IC5), self-referential (IC6). (Right) Right bar plot indicates the average correlations between EEG rhythms and the RSN time courses ($r>0.2$ are significant correlations were significant $P< 0.05$, with Bonferroni correction) (Adapted from [33]).

Rs-fMRI consists of several functional networks including the Default Mode Network (DMN), the Dorsal Attentional Network (DAN), the Control Network (CN), the Somatomotor Network (SM), the Visual Network (VN), the Auditory Network (AN) and the Salience Network (SN) (Figure 2.3) [17]. Default mode network is one of the fundamental subnetwork of resting state networks which is highly correlated with high level cognitive functions [12],[34]. Default Mode Network refers to the theory of existence of active brain regions at rest. In other words, it is called task free

functional MRI, since subjects do not perform any task with an eyes closed or open position. Moreover, the findings suggest that there are a highly correlated functional brain structures including precuneus, posterior cingulate (PCC), lateral temporal cortex, dorsal medial prefrontal cortex (vMPFC), and medial, lateral, inferior parietal cortices, cerebellum, hippocampal formation, even though the subjects do not perform any specific cognitive task [2],[18],[34],[35]. According to their findings, DMN has anti-correlation with the dorsal attention system which is associated with the information processing gathered from external sensory pathways. Based on this finding, it has been hypothesized that these two networks compete with each other in terms of functional processing [17]. To be more specific, DMN is the dynamic marker for the baseline of the internal attentional engagement since there is a BOLD signal increase during cognitive tasks, memory retrieval, episodic memory, environmental observation, during remembering, imagination, mind reading (interpretation of other people's thought) [18],[17],[36]. According to a PET study, it has been shown that the oxygen extraction fraction is uniform for the DMN. Since the ongoing fluctuations are not specific to any task, the DMN is called the indicator of baseline activity of the brain which is also present in anesthetized humans [16]. It may be inferred that it is a marker for the subject's awareness/consciousness. On the other hand, when subjects direct their attention to an external stimuli, the DMN activity reduces [12],[16]. So we can conclude that the activity of the DMN in the absence of external stimuli is higher than in the presence of external stimuli [11]. This behaviour changes in the case of other RSNs such that for the task base case, RSNs show increased correlated activity which they preserve this connectivity during resting case (though the activity decreases) [16].

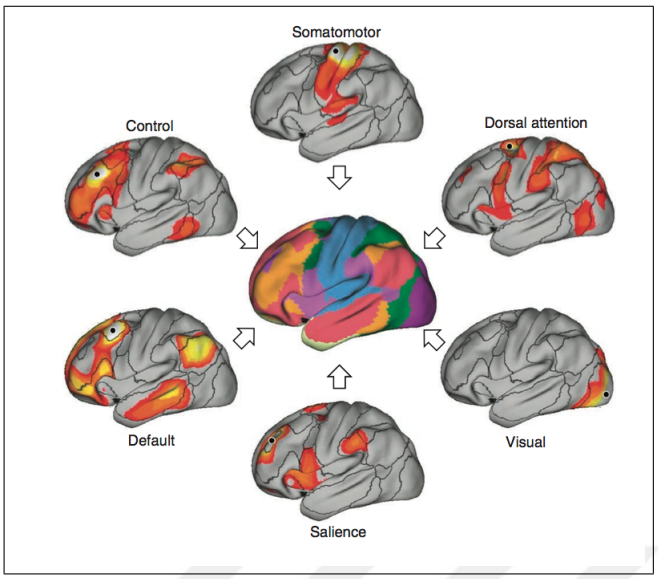

Figure 2.3 Resting state networks (Black indicates the seed region) (Adapted from [17]).

Epilepsy is a serious neurodegenerative disease which is caused by the abnormal spontaneous activity of the brain [37]. Its typical symptoms are unregulated movements, unconsciousness, and blank stare due to excessive synchronized brain activity. Incidence rate of epilepsy is assumed to be about 1 % of the entire world population [38] and about 30 % of the cases resist to drug therapy [39]. According to recent reports, in every 1000 deaths, 4 of them are caused by sudden unexplained death in epilepsy (SUDEP) [19]. Patients who are resistant to antiepileptic drugs (AEDs) have pharmacoresistant epilepsy [40]. Surgical operation has been noted as the most effective method for the drug-resistant epileptic patients [41]. Epilepsy has two types generalized and focal. In focal epilepsy, there is one focal onset, the propagation of the seizure spreads unilaterally. In generalized idiopathic epilepsy, there may be unifocal or multifocal onsets whereas the propagation of the seizure expands in bilateral brain regions [39],[42],[37]. The most common type of temporal lobe epilepsy is the mesial temporal lobe epilepsy (mTLE) whose seizure onset is thought to locate in hippocampus or parahippocampal focus. The other type is the neocortical TLE whose seizure initiation originates from lateral temporal lobe neocortex [34].

Recent EEG-fMRI studies reveal that inter-epileptic discharges (IED) and seizures have their own network topography [39]. Specifically, IEDs are the epileptic biomarkers which reflect the changes due to postsynaptic potentials of the pyramidal neurons [43]. IEDs are typically observed as sharp waves whose duration is between 70-120 ms [5]. Besides, [5] also emphasizes that the etiology of the seizure is expected to be diverse across patients or within patients. In support of this, [44] showed that two different epileptic patients having with a nearly same seizure onset zone, exhibited a unique functional connectivity patterns using intracortical EEG (icEEG). All these imply that epilepsy is assumed to be a network disease. In other words, it effects different brain regions by spreading around, so it is crucial to investigate the functional and structural network of disease to make a focal and correct localization during the surgical planning [39],[41],[45],[46],[47],[48]. Although there is no consensus on "gold−standard" for the identification of the SOZ and EZ, according to current literature icEEG is accepted as gold standard due its high sensitivity and specificity in clinical applications [38],[39],[45]. Although, it is accepted as "gold−standard", it may sometimes yield incorrect source localization results because of its limited spatial location, especially when the region where the intracranial electrodes are placed may not register any seizure onset in the case of multifocal epilepsy. According to a study, in two patients who had a non-lesional focal epilepsy were monitored with icEEG, one patient's scalp EEG data suggested a frontal lobe epilepsy (FLE), whereas the icEEG results revealed a temporal lobe epilepsy. Contrary to the other patient's scalp electrodes which is a multifocal epilepsy, the icEEG results certified a frontal lobe epilepsy [42]. At this point, the source localization for the epileptogenic zone remains elusive. To replace the need for icEEG, multimodal neuroimaging techniques should be validated by the icEEG results. Consequently, this increases the reliability of the source localization and functional navigation for the surgical planning. Additionally, the source localization technique for the multimodal imaging takes less hours than icEEG whose time duration is much more longer [49]. On the other hand, the icEEG measurements accepted as gold standard, have various complications which may result in cerebral hemorrhage and infection [50]. In the case of acquiring consistent results from both MRI and EEG, clinicians do not need to monitor icEEG. Only in the case where fMRI and EEG results do not confirm each other, another imaging modality is

required. Most of the recent studies revealed that especially in mesial temporal lobe epilepsy (mTLE), the source localization with icEEG is not required, instead of which non-invasive neuroimaging modalities can be used [49]. This finding indicates that non-invasive multimodal neuroimaging techniques can decrease the usage of icEEG.

Therefore, for the epileptic cases it is very convenient and promising to investigate the epileptogenic network when subject is at rest condition [51],[52]. It is advantageous to use resting state fMRI since most of the time patients have difficulty to perform task based experimental protocol. Additionally, it requires longer time to acquire the task based activation maps. Alternatively, the rs-fMRI is relatively easier since subjects do not need to perform any specific task. Therefore, the resting state fMRI is a useful technique for the connectivity analysis of the human brain at the stage of the presurgical planning [52]. In the case of default mode network in epilepsy, it has been shown that DMN BOLD activity significantly reduces in posterior cingulate, precuneus, and left and right frontal and parietal lobes [34]. Although the functional connectivity alteration was observed as an attenuation in DMN, the functional connectivity strengthens over the right middle frontal gyrus [34] (Figure 2.4). The reason why DMN activity increases is explained as "dynamic diaschisis". Dynamic diaschisis refers to an alteration in the brain function, particularly in order to regain the actual functionality of the brain, the healthy regions of the brain makes new connections with each other, thus it may result in hyperconnectivity [34]. As a result, it has been proposed that the loss of consciousness and awareness may be associated with the suspension of the BOLD response due to epileptic seizure [39]. Epilepsy does not only affect DMN but it also has an impact on emotional, sensorimotor, attention, executive motor control networks of the human brain [34],[46]. The functional connectivity decreases in dorsal attention, auditory and sensorimotor networks [46].

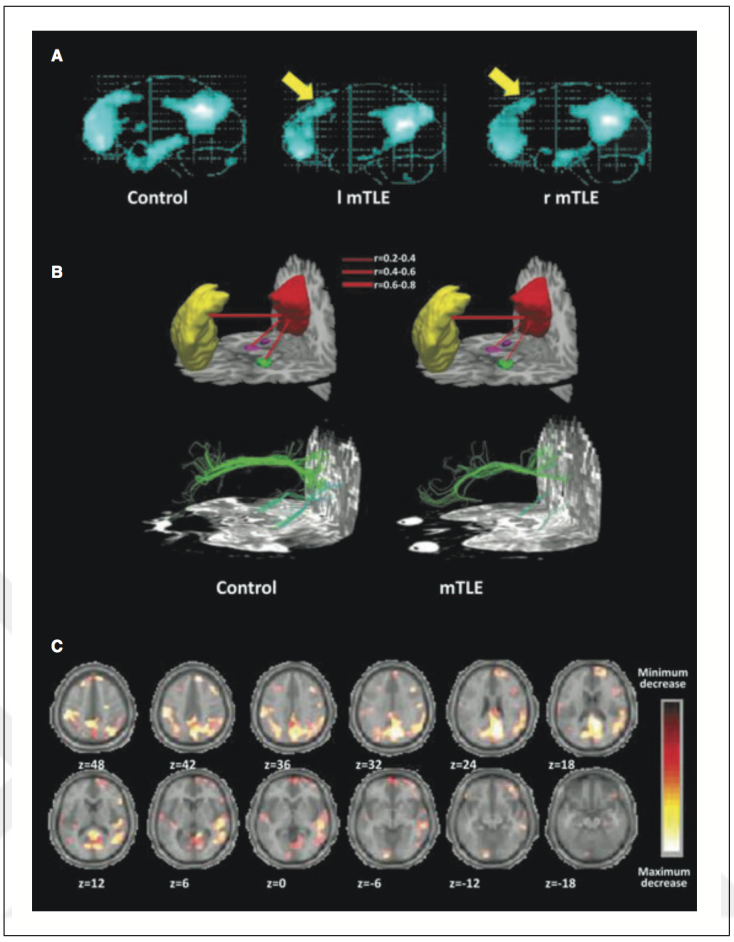

Figure 2.4 The connectivity discrepancies of the default mode network (DMN) activity between controls and temporal lobe epilepsy. (A) DMN comparison of control subjects with right and left temporal lobe patients. (B) The main anatomical areas including precuneus/ posterior cingulate cortex (in red) and medial prefrontal cortex (in yellow), right (in magenta), and left (green) mesial temporal cortex in DMN where connectivity decreases/increases through fMRI and diffusion tensor imaging which measures the reconstruction of the white matter fiber bundles. (C) fMRI maps including the anatomical regions whose activity decreases during the propagation of interictal epileptic activity under simultaneous fMRI and EEG monitoring (Adapted from [34]).

According to a DMN study [52], it has been shown that default mode network may infer the post surgical outcome of the patient in terms of cognitive impairment. The results reveal that the left temporal lobe epilepsy patients who have higher connectivity between posterior cingulate cortex and left hippocampus (HC) have greater

memory decline after the resection of the left temporal lobe in the post surgical phase, whereas if there is a higher connectivity between the PCC and contralateral HC, this ends up with either no memory decline or less memory decline. To understand the relation between temporal lobe epilepsy and DMN, [53] investigated DMN using ROI based partial correlations in epileptic patients through fMRI. Subjects were either right or left temporal lobe epileptic patients with rare interictal epileptiform discharges. ROI seeds were chosen as centered on posterior midline (Rsp (retrosplenial cortex)/PCUN (precuneus)) region (x=0, y=-51, z=32) and the ventromedial pre-frontal cortex (anterior) (vmPFC; x=3, y=60, z=-1) in the standard MNI space and then these ROIs projected from MNI space to each subject's individual brain space. Subject-wise partial correlations between seed regions and all the voxels in the brain were calculated. Regardless of the lateralization, the connectivity between the posterior DMN (Rsp/PCUN) and the anterior portions (medial frontal) of the DMN significantly decreased bilaterally (Figure 2.5 and Figure 2.6).

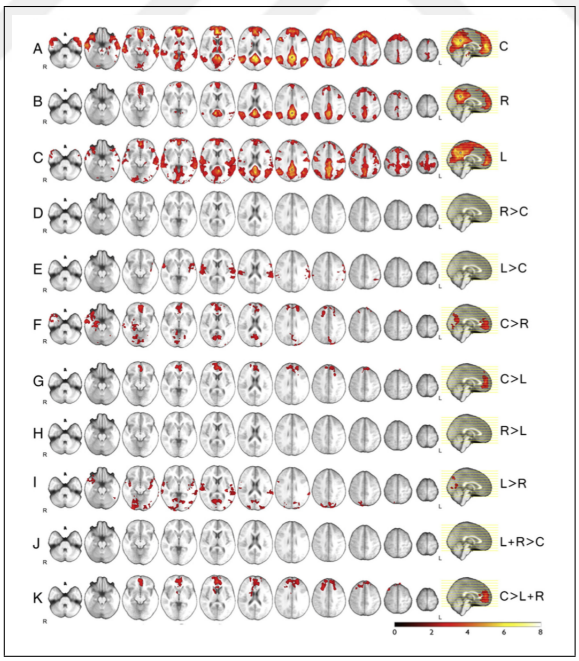

Figure 2.5 Partial correlation activation maps between groups based on posterior seed region, colour bars represent z-scores (z>2.0, p=0.05), C=control; R=right TLE; L=left TLE (Adapted from [53]).

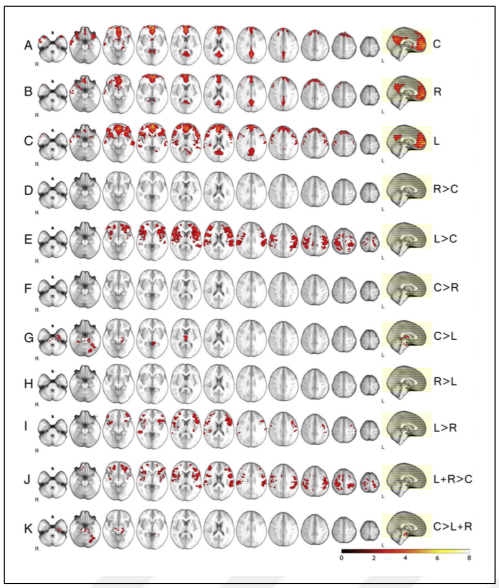

Figure 2.6 Partial correlation activation maps between groups based on anterior seed region, colour bars represent z-scores (z>2.0, p=0.05), C=control; R=right TLE; L=left TLE (Adapted from [53]).

[54] also examined the interregional brain connectivity in temporal lobe epilepsy patients using partial correlation. Both correlation and partial correlation coefficients were computed. According to direct connectivity results, right basal-frontal (RBF) was a driving source on behalf of others, there was a direct relation between RBF and the right polar temporal (RPT), RBF and left basal frontal (LBF), whereas RPT and LBF did not have statistically significant partial correlations. On the other hand, RBF, LBF and RPT comprised statistically significant connections as a result of marginal correlation coefficient computation (Figure 2.7).

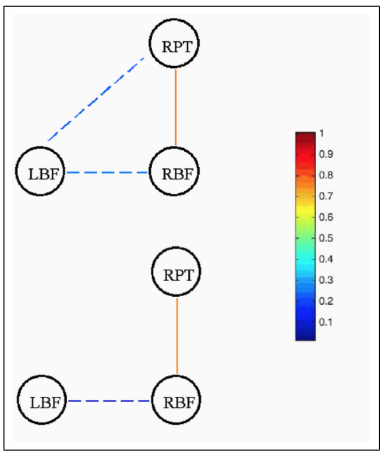

Figure 2.7 Correlations (top) and partial correlations (bottom) that are significantly different from zero ($P<0.05$). Colorbar represents the strenght of the functional relation (Adapted from [54]).

Functional connectivity patterns are susceptible to a high functional variability due to the individual differences in the human brain [55]. The frontoparietal control, the attentional, the default mode networks showed highly varied functional connectivity patterns whereas the vision and the sensorimotor networks showed less variance in the healthy humans according to the 7-resting state networks in [56],[57]. This variability is stemming from the discrepancies in neuroanatomy and function which are observed in human cognition and behaviour [57]. The inter-individual differences can be observed in Figure 2.8 and the seven resting-state networks is given in Figure 2.9.

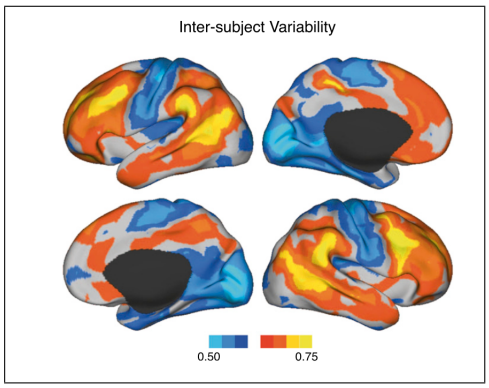

Figure 2.8 Inter-subject variability in resting-state functional connecitivity of the healthy brain. The warm colors represent the regions that are higher than the global mean, cool colors are shown the values lower than the global mean (Adapted from [57]).

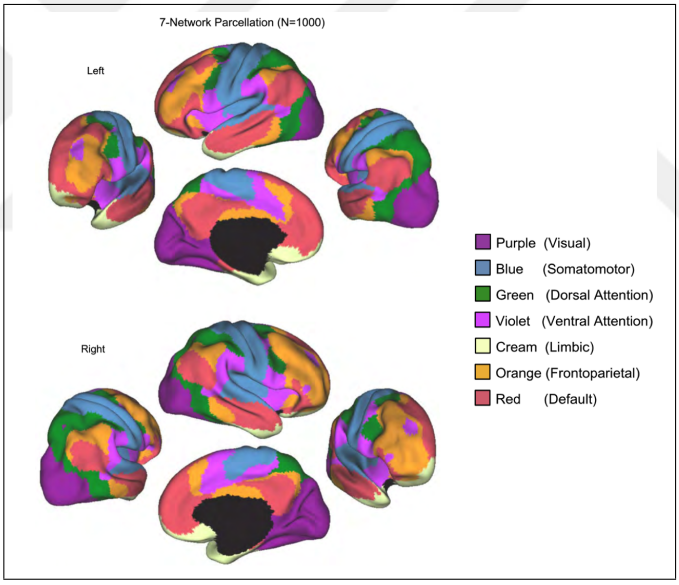

Figure 2.9 The seven resting-state networks (Adapted from [56]).

2.1.3 Computational Methods for Functional Brain Connectivity

Functional connectivity is defined as the temporally correlated ongoing fluctuations between different brain regions to investigate the brain organization. Therefore, functional connectivity mainly sheds light on the interactions between different brain regions by mapping the intrinsic functional brain activity. To that extent, it is one of

the fundamental techniques in both task based and resting state fMRI. Resting state fMRI refers to low frequency intrinsic fluctuations while subject is at rest [18]. From the methodological point of view, by making use of EEG and fMRI modalities, functional connectivity has been investigated through seed-based connectivity analysis using linear/nonlinear correlation and partial correlation coefficients, Independent Component Analysis (ICA), General Linear Model (GLM), Principal Component Analysis (PCA) and Clustering Methods [8],[58],[59]. In particular, ICA and seed based methods are the most commonly applied functional connectivity techniques as well as clustering algorithms [4]. The data processing pipeline for fMRI and EEG-fMRI analysis techniques is shown in Figure 2.10 and 2.11, respectively.

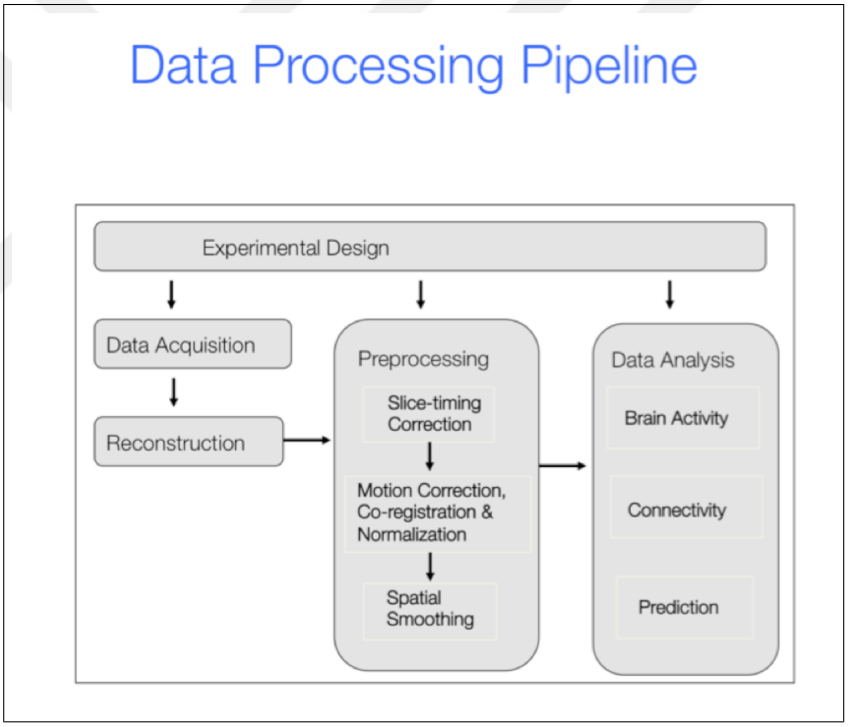

Figure 2.10 fMRI data processing pipeline (Adapted from [8]).

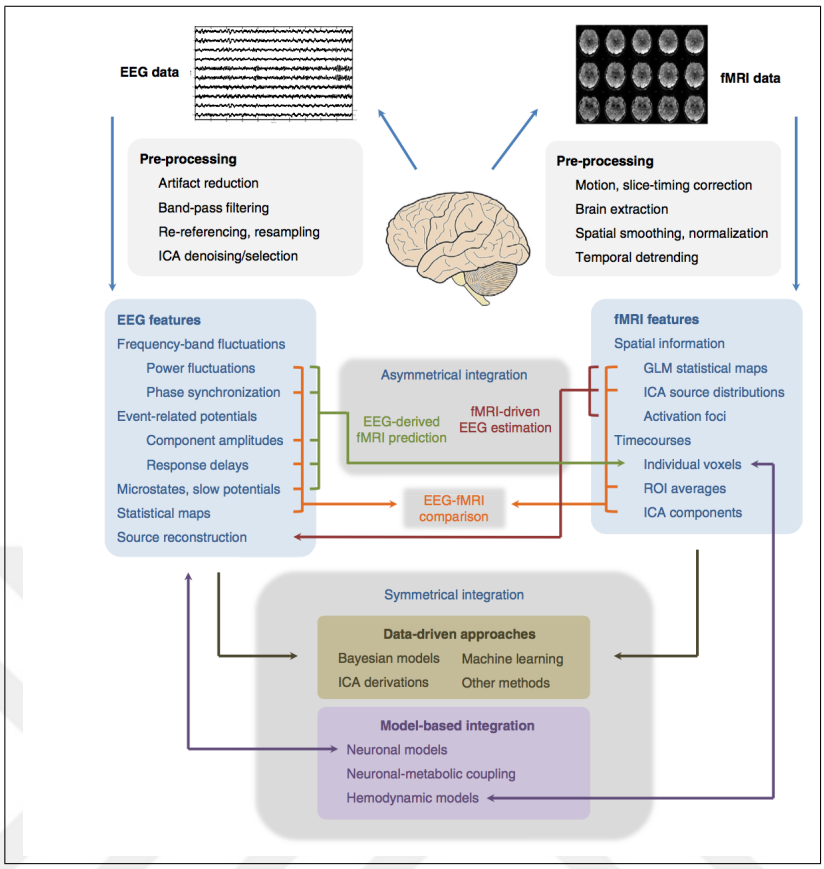

Figure 2.11 EEG-fMRI data integration and analysis (Adapted from [60]).

2.1.4 Data-Driven Approaches and Neuroimaging Applications

Seed based connectivity usually illustrates a metric which elucidates the relation between different brain regions whereas ICA results in providing three different connectivity metrics including total connectivity, connectivity within networks and connectivity between networks. Nonetheless, seed based results can be defined as the combination of ICA based connectivity within networks and connectivity between networks [4]. Independent Component Analysis (ICA) expresses the BOLD response when there is no a priori knowledge or hypothesis. In other words, ICA is a data-driven technique to analyze the whole brain data in terms of its functionality without a priori knowledge about the task which activates the brain. To sum up, ICA decomposes the data into spatially or temporally independent components by maximizing the non-gaussianity or minimizing the mutual information among components [18],[46],[59]. In

general, the types of signals can be grouped into two classes which are of interest and not of interest. Task-related and function-related signals comprise the signals of interest. The function-related signals represent the similarities between voxels that belong to the specific domain. The task-related signal which is highly correlated with the data, represents the waveform of the paradigm. The signals of not interest include physiology-related, motion related, and scanner-related signals. Physiology-related signals such as breathing and heart rate arise from the brain ventricles or brain regions with large blood vessels. On the other hand, motion-related signals such as patient movement or brain movement may cause large abrupt changes on the data [61]. The function of the brain basically works on two principles localization and connectionism. Namely, localization implies each psychomotor function is carried out in a set of brain areas (region of interest) and these areas may have a connection with each other both structurally and functionally [62]. As a result, ICA simply separates the observed data into set of independent variables such that signal observed at a given voxel is modelled as a sum of the contributions of all the independent components. ICA is solved as follows:

$$X = A * S \tag{2.1}$$

where X is an observed m-dimensional data vector, S is an n-dimensional random vector (source matrix) whose components are assumed mutually independent, and A is a constant $m \times n$ mixing matrix, both A and S are unknowns to be estimated [63]. This algorithm iteratively determines the mixing unknown matrix S by solving

$$S = A^{-1} * X \tag{2.2}$$

until the convergence of independence among components. First of all, the data become uncorrelated by using prewhitening, afterwards, the mixing matrix A and its inverse is estimated by maximizing the non-gaussianity or minimizing the mutual information between components [59].

ICA has been used in many neuroimaging applications including RSNs including DMN. For instance, [64] applied ICA on resting state fMRI data in healthy participants and patients with reversible and irreversible coma following cardiac arrest to investigate

the role of DMN on functional connectivity. According to their hypothesis, the connectivity over DMN is not changed in patients in reversible coma whereas it is altered in those in patients with irreversible coma. Significant activations regarding DMN in healthy controls as well as in reversible coma patients are given in Figure 2.12 (A) and Figure 2.13 respectively, whereas for irreversible comatose patients, there is no significant result in terms of functional connectivity within DMN (Figure 2.12 (B)). All these findings suggest that the DMN mainly reflects the brain organization in terms of consciousness. But it does not purely represent awareness, it may rather be required for consciousness [64].

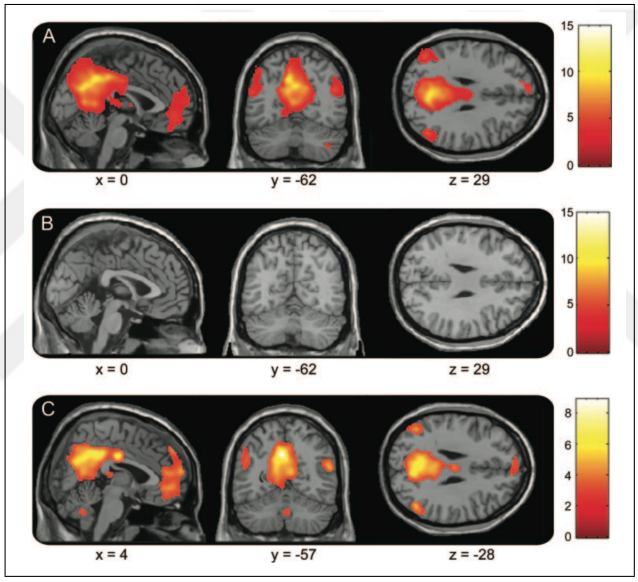

Figure 2.12 (A) Default Mode Network including the posterior cingulate cortex (PCC)/precuneus, bilateral temporoparietal junctions, and medial prefrontal cortex in control subjects as a result of ICA. (B) Functional connectivity in DMN in irreversible coma patients. (C) Functional connectivity map in control subjects vs. irreversible coma patients (Adapted from [64]).

In comparison wtih ICA, the clustering methods still need to select ROIs before the computation of clusters. Furthermore, ICA considers all of the brain voxels for the computation of functional connectivity maps [18]. At this point, ICA is advantageous. However, it has been shown that in results of seed based, clustering and ICA techniques, there are consistently numerous overlapping regions implying similar brain activations. For instance, in ICA results, the activations observed in the DMN and the primary

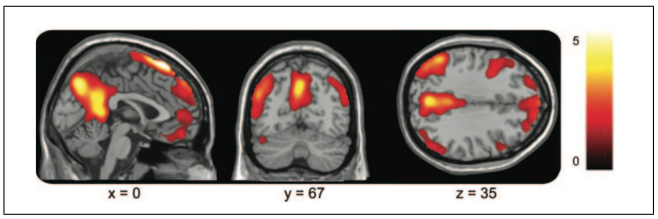

Figure 2.13 (A) Group functional connectivity map of DMN in reversible coma patients (gained consciousness) (Adapted from [64]).

motor cortices are also validated by both clustering and seed based methods [13]. As a second advantage of ICA, the noisy signals can be detected as separate components of ICA without performing other preprocessing steps. Although ICA has some advantages, it also has some drawbacks. First of all, the number of components should be pre-defined but there is no consensus on selecting them and the results should be visually inspected by the researcher. As a consequence, this may cause a arbitrary selection of components since different researchers may select different components as a noisy and functional networks [18],[65]. One of the most common methods to map the functional connectivity including RSNs is seed-based analysis [32]. To calculate functional connectivity, mainly two types of seed based techniques are used; ROI based and voxel based. For seed based analysis, the fundamental measure to compute the synchronous relations such as correlation, partial correlation or regression among different brain regions is the covariance matrix [18]. The calculation for the seed based functional connectivity between voxel 1 and the seed voxel 2 can be defined as follows:

$$C_{SB}(x_1, x_2) = \frac{\sum_{t=1}^{T} S(x_1, t)S(x_2, t)}{\sqrt{\sum_{t=1}^{T} S^2(x_1, t)}\sqrt{\sum_{t=2}^{T} S^2(x_2, t)}} \tag{2.3}$$

where S(x,t) is the demeaned BOLD fMRI signal from voxel x at time t and T is the number of time points in the experiment [4]. [4] investigated the differences and similarities between seed based temporal correlation and ICA through various paradigms including simulations, visual, visua-motor and resting. While performing the comparison, since preprocessing stage is slightly different in seed based and ICA techniques, they applied different combinations which were seed based connectivity with conventional seed based preprocessing (CSBP), ICA with conventional ICA preprocessing,

and seed based connectivity with conventional ICA preprocessing. The seed based connectivity with CSBP asserts similar functional connectivity maps with ICA in comparison to seed based connectivity with conventional ICA preprocessing (including pre-whitening and dimensionality reduction after removing the physiological signals), since there is an information loss due to dimensionality reduction which is not justified as a neuroscientific proof of concept. As an important finding, ICA based sum of within network connectivities (WNCs) and between network connectivities (BNCs) are the same as seed based connectivity results. But for the coactivated task based results, seed based connectivity basically provides information that is specific to the experiment, besides, it does not explain the exact relation between instrinsically connected networks. As opposed to this, ICA decomposes the data into several components which provide functional information about all distinct networks. They concluded that seed based correlation was the GLM-based computing whose input was the seed voxel time course. Therefore, seed based functional connectivity yields a "model" whose input is directly related to a seed voxel. On the other hand, ICA based functional maps provides both "states" of the human brain and their temporal dependencies.

Seed based methods are mainly categorized into two that are seed-to-whole brain connectivity and seed-to-seed functional connectivity. In the case of seed-to-whole brain connectivity, first of all, the seed region is defined and the average of all voxel time series is calculated within that region. Thus, the correlation coefficients are computed between this averaged time series and each voxel in the brain image. The Pearson's correlation between two time series is calculated as follows [66]:

$$r = \frac{cov_{XY}}{S_X S_Y} = \frac{\sum_{i=1}^{n}(X_i - \bar{X})(Y_i - \bar{Y})}{\sqrt{\sum_{i=1}^{n}(X_i - \bar{X})^2}\sqrt{\sum_{i=1}^{n}(Y_i - \bar{Y})^2}} \tag{2.4}$$

where X and Y are brain activity time series, n is the number of time points, and $\bar{X}$ and $\bar{Y}$ are the mean time series, S is the time series standard deviation, cov_{XY} is the covariance. As a final step, r-coefficients are converted into z-scores via Fisher's transform. In this technique, the challenging part is choosing the seed region, since it is not only significant in terms of functional connectivity results, but it is also critical for the explanation of these maps. Regardless of anatomically defined or atlas-based seed

regions or task-based functionally defined regions, seed regions are used to illustrate the functional connectivity maps. For the anatomically defined or atlas-based seed regions, based on an anatomical region of interest or reference (standardized) atlas, subject-wise seed region is defined. On the other hand, task-based functionally defined seed regions can be identified as a predefined volume which takes the Talairach coordinate of task based activation from previous studies as a center point. ROI-based functional correlation maps illustrate the interaction between apriori defined regions. Besides these fundamental approaches, an alternative method is the computation of partial correlation coefficients which illustrate the direct relation among different brain regions [18].

Although both ICA and seed based methods have some disadvantages, they mainly express the brain organization in terms of functional networks [65]. Nevertheless, to perform detailed analysis of functional connectivity, partial correlation coefficients have been calculated among different brain regions. It indicates the direct functional relation between different anatomical regions by regressing out the effect of other regions. In that extent, [27] explained the data driven measure called the partial correlation coefficient in terms of both theoretical and practical aspects. In this study, the partial correlation coefficients (also referred as conditional coefficient) between two regions i and j denoted by $\prod_{ij}$ are defined as:

$$\prod_{ij} = Corr[x_i, x_j | x_{R \setminus ij}] \tag{2.5}$$

Set

$$\gamma = (\gamma_{ij}) = \Sigma^{-1} \tag{2.6}$$

where Σ^{-1} is the inverse covariance matrix (also called precision matrix) of BOLD time series data. Given γ, the partial correlations for two distinct regions are computed by:

$$\prod_{ij} = -(\gamma_{ij}) / \sqrt{\gamma_{ii}\gamma_{jj}} \tag{2.7}$$

In this study, it has been argued that the partial correlation is closer to effective connectivity than the marginal correlation coefficient since it provides direct functional relation maps through the graphical illustrations. Thus, it basically gives an idea about the plausible connectivity pattern before the computation of effective connectivity. As opposed to other effective connectivity matrices (Dynamical Causal Modeling or Structure Equation Modeling), it does not require a priori input to the model. It is not possible to find directionality without prior information for such model "A->B->C" but partial correlation can be converted into effective connectivity. By the partial correlation it should be predicted that A and C do not directly depend on each other, so the resulting model generated as "A-B-C" instead of "A->B->C". This inference implies that there cannot be such a model "A->B<-C", since in this collider model, there will be a negative partial correlation coefficient between the nodes A and C as clearly explained in [67], without eliminating "A->B->C", "A<-B<-C", "A<-B->C". As a practical application, they proposed a bayesian model to predict the true partial correlation coefficients about 6 ROIs in [27]. As a result of hand movement task, there is a high correlation between the two sensorimotor cortices (RSMC and LSMC), the two supplementary motor areas (RSMA and LSMA), and the two premotor areas (RPMC and LPMC). According to the results on partial correlation coefficients, they have obtained an important finding regarding the role of premotor cortex over other structures, that the activity in the sensorimotor cortices and premotor contralateral to the hand movement were highly correlated compared to those in the ipsilateral hemisphere. They concluded that partial correlations were more robust than marginal correlation coefficients since it eliminated the effects of other variables over a large scale. A detailed information regarding the causal inference of partial and marginal correlations can be found in Figure 2.14 [67].

As a model free approach, partial correlation does not only reveal the functional connectivity but it is also associated with structural connectivity, namely the white matter tracks (connected axons) that connects one region to another [68]. In literature, it has been argued that structural connectivity implies functional connectivity whereas the reverse case may not happen all the time. When there is a functional connectivity between different brain regions, they do not have to be necessarily struc-

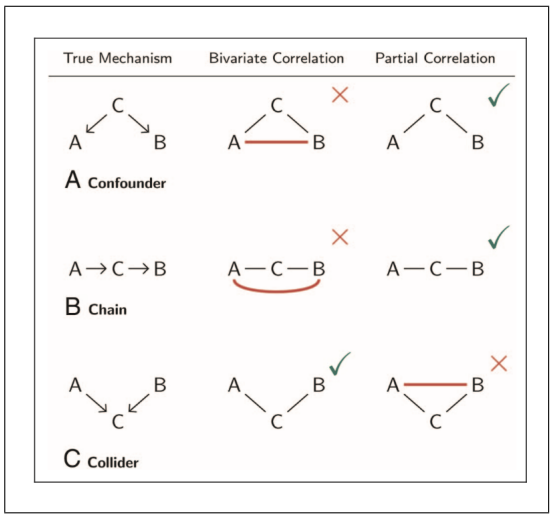

Figure 2.14 The comparison between bivariate and partial correlations in prediction for the causal inference (Adapted from [67]).

turally connected [69]. For instance, although the left and right central primary visual cortex are functionally correlated, these regions are not structurally connected ("central V1 callosal connections are not present in Old World primates", p.832) [17]. On the other hand, [13] noted that according to the results of another study, almost all of the functionally connected resting state regions have also structural connections by established white matter tracts. As a result, the entire relation of structure to function still remains unsolved [13].

Functional connectivity studies mainly reveal temporally correlated distinct brain regions for both task relevant and RSNs. As a fundamental RSN, the DMN takes a step forward to its ability of being a biomarker for abnormalities of human brain [36]. For the DMN, the precuneus (Pc/PCC), the so called Heteromodal Association Areas (HAAs), implying the connection among a large number of advanced anatomical regions, has been found to be the main hub by the graph theory analysis [70]. According to [36], as an indicator of the effective connectivity, partial correlations were computed through different ROIs during resting state and task based fMRI. Thus, this method does not require a priori information as well as excluding the bias to find the modulation of different brain relations directly. They explained that since the pairwise correlation coefficients did not consider the covariance matrix of whole

DMN, there was a considerable amount of information loss. To reveal this methodological pitfall, they applied partial correlations which were measures for excluding mutual dependencies from common driving sources of all structures of DMN. They gathered the fMRI signal ROIs from nine brain regions including precuneus/posterior cingulate cortex (pC/PCC), left and right inferior parietal lobe (lIPL, rIPL), dorsal and ventral medial prefrontal cortex (dmPFC, vmPFC), left and right temporal cortex (lTC, rTC) and left and right medial temporal lobes (lMTL, rMTL). For the first level of analysis, ICA decomposed the fMRI data into 60 components in individual basis. As a second level, based on these spatial maps the ROIs were chosen and partial and marginal correlations were computed over the ROIs that were aforementioned at the group level. As a result of the correlation coefficient computation, they reported that all components of DMN were highly correlated with each other at rest. On the other hand, according to the partial correlation results, as a prominent finding, Pc/PCC has been found to be a unique core structure for DMN in terms of having a large number of direct interactions with other regions except for rMTL. The results revealed that there was a strong functional connectivity between the pC/PCC and the left inferior parietal cortex as well as between the dorsal part of the medial prefrontal cortex. As an important note, although there was a strong interaction between left and right MTL during rest, their connectivity decreased with the rest of the DMN. This implied an independence from the rest of the regions in DMN. For the results of verbal n-back test, there was a large scale connectivity reduction within the DMN, though its overall functional interaction within itself was preserved. From the physiological point of view, being consistent with the previous literature, the finding regarding the pC/PCC confirms that it is the anatomic region which regulates self-consciousness implying the process of self-referential mental thoughts during rest. As a supporting evidence from the PET studies, it has been confirmed that this region (pC/PCC) has a high metabolic activity when compared to others. The comparison of correlation with partial correlation in terms of their coefficients is given in Figure 2.15.

To investigate the functional relation between different brain regions, covariance, precision or correlation matrix estimation is required to be computed [2],[71]. The conventional method for assessing the functional connectivity is the calculation

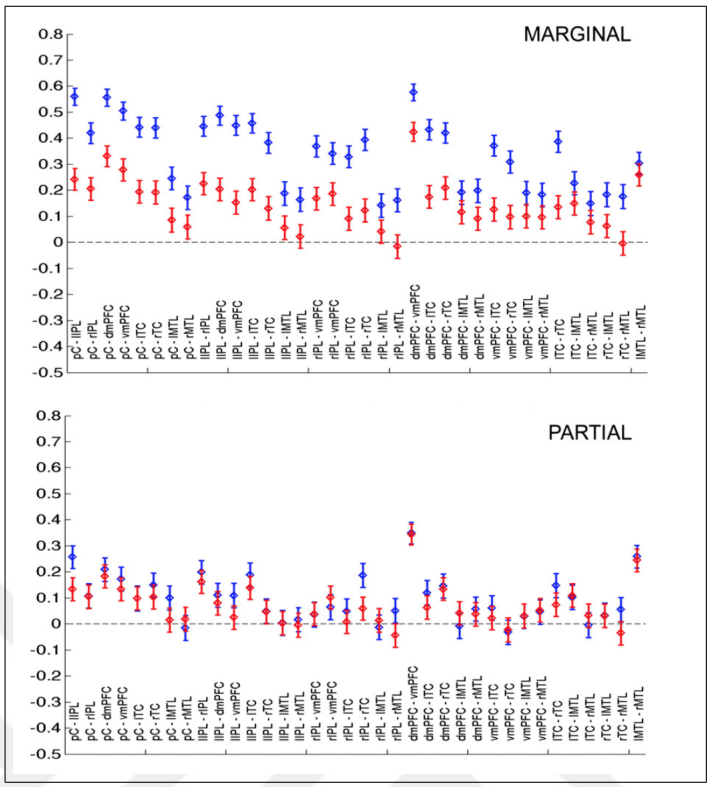

Figure 2.15 The connectivity results of the default mode network (DMN) activity of healthy subjects during resting state fMRI (blue) and a working memory task (red) (Adapted from [36]).

of correlation coefficients. However, the correlation coefficients also contain the effect of other regions throughout the brain. In order to assess the direct relations within the brain, partial correlation coefficient has to be computed. To find partial correlations between different brain regions, first the inverse of covariance matrix needs to be calculated. The non-diagonal elements of inverse covariance matrix gives an idea about the partial correlations, namely if the elements of inverse covariance matrix is zero, then this implies that partial correlations are also zero inferring that the data points are conditionally independent from each other [26]. However, if the number of time points (n) during an fMRI scan is considered, it is relatively low compared with the number of voxels or ROIs (p) within the brain. The number of pre-selected ROIs become limited since when p>>n, the sample covariance matrix has a large number of zero eigenvalues. Thus, it becomes rank deficient and cannot be inverted because of the curse of dimensionality [28],[68],[72],[73],[74]. Instead of computing the direct in-

version, there has been different methods proposed including pseudo-inverse, L-1 norm, L-2 and L1-2 regularization (called Elastic net regularization), Ledoit−Wolf covariance regularization and Bayesian approaches [26],[68],[73].

In the case of pseudo-inverse computation of a matrix, the non-zero eigenvalues of the sample covariance matrix are used. However, as n→p, the difference between the pseudo-inverse and the inverse covariance becomes significant, since smallest non-zero eigenvalues which are approaching zero, used to construct pseudo-inverse of the sample covariance matrix. To solve this limitation, [74] examines "Random Matrix Theory" which confirms the discrepancy between the inverse and the pseudo-inverse covariance is a feature of the large population matrices. They state that "The sample covariance eigenvalue density is self-averaging. That is, the eigenvalue density from a single large-sample covariance matrix is well-approximated by the average eigenvalue density obtained from an ensemble of such sample covariance matrices" (p.1473). As a result, rather than computing the pseudo-inverse of all the data set, it is more convenient to partition it into small data sets and calculate their pseudo-inverse inverses. As an application of random matrix theory on fMRI data, [28] computed partial correlation coefficients between a seed region and each target brain voxel by using pseudoinverse covariance matrix. Partial correlation coefficients are computed not only for removing the global artifacts regarding head movement, cardiac pulsation but also functional connectivity on resting state fMRI data. As a result, the proposed algorithm outperforms the existing methods in terms of high sensitivity, specificity and accuracy as well as providing additional strong connections on default mode network and more robust identification of connectivity with left and right medial temporal lobe regions compared to the global signal regression method. Random subspace method is advantageous in terms of providing high accuracy of inverse covariance matrix since the data is divided into many number of submatrices, the sample-to-feature ratio becomes high as opposed to original data set. The novel random subspace method for functional connectivity (RSMFC) algorithm is given in Figure 2.16. Both methods are applied on rs-fMRI data by selecting the posterior cingulate cortex (PCC) as a seed ROI in order to compute the whole-brain functional connectivity map. Two uncorrelated data sets are constructed including bilateral medial prefrontal cortex (mPFC), angular gyrus regions (AG), and

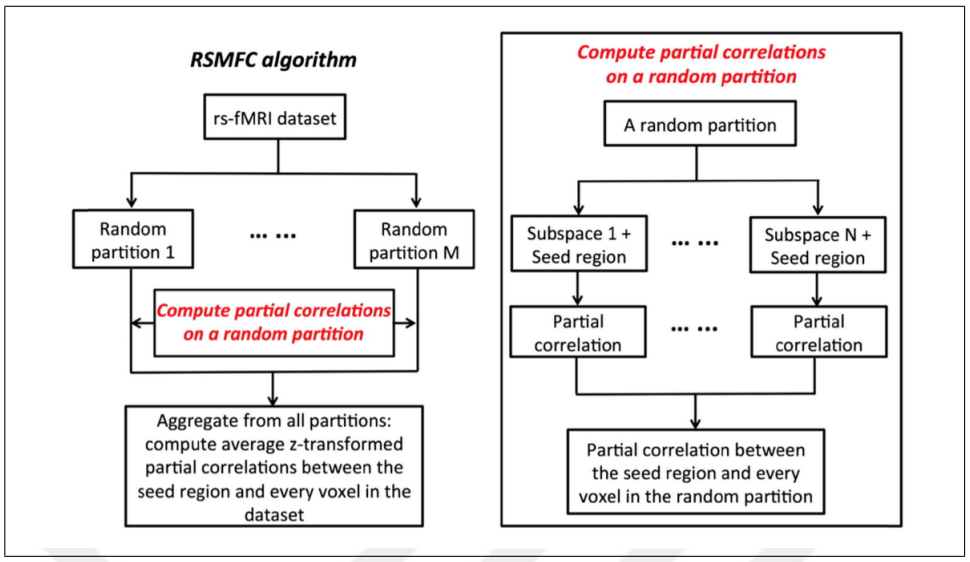

Figure 2.16 The novel random subspace method for functional connectivity (RSMFC) algorithm (Adapted from [28]).

medial temporal lobes (MTL) for the first and, lateral fronto-parietal regions for the second. RSMFC algorithm detects the connections as uncorrelated networks, whereas global signal regression method finds an anti-correlation between these two networks. Although the main hubs of the DMN are visible in the results of both algorithms, the anatomical specificity of RSMFC is higher than that of the global regression. As a result, RSMFC is a promising approach to investigate the functional brain maps. For a non-full-rank matrix A, the pseudo- inverse A^+ is given by [74] as:

$$A^+ = (A^T A)^{-1} A^T \tag{2.8}$$

where $AA^+ = I$.

The pseudo-inverse, A^+ minimizes

$$\|AA^+ - I\|_F \tag{2.9}$$

where F is the Frobenius norm

$$\|X\|_F^2 = \sum_{ij} X_{ij}X_{ji} = trXX^T \tag{2.10}$$

The pseudo-inverse of data matrix D can be calculated as follows [74]: For p*n centered data matrix D which is normalized as,

$$D = (E_1 - \mu, E_2 - \mu, E_3 - \mu, ..., E_n - \mu) \tag{2.11}$$

where μ is the sample mean and E_μ, $\mu = 1, 2, ..., n$. The sample covariance matrix $\hat{C}$ is given as

$$\hat{C} = n^{-1}DD^T \tag{2.12}$$

For n $<$ p, the sample covariance C is singular, and so the pseudo-inverse of C denotes as $\hat{C}^+$ which is an estimator of C^{-1} should be calculated.

$$\hat{C}^+ = nD(D^TD)^{-1}(D^TD)^{-1}D^T \tag{2.13}$$

L1-norm regularization is also used to compute the inverse covariance matrix. It has several advantages including imposing sparsity and dispensable statistical thresholding while detecting significant relations since insignificant connection values are set to zero. Although it has several advantages, it has some drawbacks. To be more precise, if the number of observations is less than the number of nodes, the identification of the number of network connections is limited to the number of observations. Besides, if the correlation coefficients are high in pairwise manner, L1 can only detect a sub-network of these connections. Since the spatial correlations between these brain regions are high and they are near to each other, the L-1 norm becomes insufficient in terms of regularization [26]. L1-norm is computed as;
Let $S \succeq 0$ be a given empirical covariance matrix, for data drawn from a multivariate Gaussian distribution. Let the variable X be the estimated inverse covariance matrix.

The L1-norm regularization solves the maximum likelihood problem as

$$\max_{X \succ 0} \log \det X - \langle S, X \rangle - \rho \|X\|_1 \tag{2.14}$$

where $\langle S, X \rangle = trace(SX)$ is the the scalar product between two symmetric matrices S and X, X and the term

$$\|X\|_1 := \sum_{X=i,j} |X_{ij}| \tag{2.15}$$

penalizes nonzero elements of X. Here, $\rho > 0$ adjusts the degree of the penalty [75]. To solve this problem, [26] combines L1-norm regularization with L2-norm regularization which results in column-wise sparsity. By imposing L2 norm regularization that is sum of squares of weights, the second limitation of L1 norm regularization is thought to be solved. L1-2 norm regularization is applied in order to estimate the sparse partial correlations. This algorithm is applied on resting state fMRI data with 90 cortical and subcortical structures that are obtained from anatomical templates. Elastic net regularization outperforms L1-norm results in terms of high sensitivity and accuracy. As a result, the novel findings of elastic net result in identifying of a high degree of inter-hemispheric links between homologous anatomical regions, distinct ventral and dorsal stream pathways, and a major hub precuneus in the posterior medial cortex.
[68] recently investigates the inverse covariance matrix via Ledoit-Wolf covariance regularization. Let $X \in R^{T*M}$ be BOLD time-series, where T is number of time points and N number of regions, the sample covariance matrix is given:

$$\hat{\Sigma} = \frac{1}{T}(X - \bar{X})^t (X - \bar{X}) \tag{2.16}$$

When $\hat{\Sigma}$ is not invertable, Ledoit-Wolf covariance regularization solves:

$$\hat{\Sigma} = (1 - \alpha)\hat{\Sigma} + \alpha\Delta \tag{2.17}$$

where α is a tuning parameter and Δ is the shrinkage target that makes covariance invertible. Partial correlations are computed in both eyes closed and eyes open resting

state conditions by using Ledoit-Wolf covariance regularization. Two different data sets are generated. For the first group 36 ROI are selected including 5 RSNs, for the second group 236 ROI are detected including 12 RSNs including somatomotor, cingulo-opercular, auditory, default mode, parietal encoding/retrieval, visual, fronto-parietal control, salience, subcortical, ventral attention, dorsal attention, and cerebellum networks. When full and partial covariance matrices are computed, partial covariance matrix is affected by the homotopic functional connectivity, implying that it provides some distinct features regarding the brain structure. The full covariance is partially determined by the shared variance of the RSNs which was removed by partial covariance. As a remarkable highlight, although it has been hypothesized that partial correlations reflect structural connectivity, they find out that it does not only provide information on white matter tracks, but it also gives an insight about brain states modulated by using eyes open and eyes close conditions. There is a dramatic change in the full correlation functional connectivity. However, for a few ROIs' functional connectivity is changed in the case of partial correlation. As a result, the altered functional connectivity in partial correlation is more focal when compared to full covariance alterations, provided with a less inter-subject variance.

3. METHOD

3.1 Methodology

3.1.1 Research Population

A total of nineteen right/left TLE patients (13 Females, 6 Males, age: 28.47 ± 11.36 years; age range $14-52$) were diagnosed according to the International League Against Epilepsy (ILAE) guidelines. Nineteen healthy subjects (13 Females, 6 Males, age: 24.89 ± 5.38 years; age range $20-40$) were enrolled as gender ($p = 1$), age ($p = 0.22$) and mean signal-to-noise (SNR) ($p = 0.86$) ratio matched control group after having signed the informed consent. In order to eliminate the susceptibility due to motion, the motion parameter (mean relative head displacement) between groups was compared and no difference was detected between the groups ($p > 0.05$). Each participant underwent through three separate fMRI sessions after having signed the informed consent in Xuanwu Hospital of Capital Medical University. All patients were medicated. None of the subjects had any other neurological or psychiatric disorder. This study was approved by Xuanwu Hospital of Capital Medical University Ethics Committees. Demographic information is given in the appendix.

3.1.2 Data Collection

Functional data were acquired using 3T Siemens Scanner with a 32- channel head coil at Xuanwu Hospital of Capital Medical University. The echo planar imaging functional was collected as contiguous 124 volumes for each subject (TR = 3000 ms; TE = 30 ms, FA = 90°, FOV =64 mm; voxel size = $3 \times 3 \times 3.48$ mm^3). The anatomic $T1-$weighted images were collected with (TR = 1600 ms; FOV = 256 mm, TE=2.15 ms, TI=800 ms, FA=9 °; voxel size=$1 \times 1 \times 1$ mm^3). Participants were instructed to stay awake inside the scanner with their eyes closed.

3.1.3 Data Analysis

Resting state fMRI data were preprocessed with FSL (https://fsl.fmrib.ox.ac.uk /fsl/), FreeSurfer (http:// surfer.nmr.mgh.harvard.edu) and SPM (https://www.fil.ion. ucl.ac.uk/spm/, Wellcome Trust Centre for Neuroimaging, London, England) software. The first 4 volumes were discarded to ensure magnetic stabilization. The resting state functional images were, slice time corrected, motion-corrected using rigid body transformation of the FSL software and bandpass filtered ($0.01 - 0.08$ Hz). As a last step, the head motion, the averaged ventricular signal, the averaged white matter signal and global signal regression were all regressed out. For each individual, a surface representation of the cortex from the structural image was reconstructed and registered to a common spherical coordinate system using FreeSurfer. Each individual's functional image was registered to the structural image based on boundary-based registration [76]. The functional images were also registered to a common spherical coordinate system via sampling from the middle of the cortical ribbon in a single interpolation step [56]. The resting-state BOLD fMRI data represented the entire cortical surface of each subject with a total of 5124 vertices, 2562 being in each hemisphere. The detailed description of the preprocessing pipeline is explained in [56].

3.1.3.1 Inter-subject Variability Analysis. To assess the variability defined in Eq. 3.2 and Eq. 3.3 with regard to the epileptic patients and the healthy controls, a previously published study [57] was replicated. In the first phase of the two stage algorithm, we calculated the intra-subject variability, and in the second phase, the inter-subject variability from which we regressed out the intra-subject variance. To calculate the intra-subject variability, the Pearson's correlation coefficients over all vertices were computed resulting in a final correlation matrix (5124×5124). In the first step, by taking each of voxel as a seed, we calculated the mean similarity (Eq. 3.1) and intra-subject variability across sessions (Eq. 3.2, Eq. 3.3). As the final step, we computed the inter-subject variance by regressing out the intra-subject variability using the general linear model (Eq. 3.4, Eq. 3.5).

Similarity is defined as;

$$R_i(t) = E[corr(F_i(s_p, t), F_i(s_q, t))] \tag{3.1}$$

where $F_i(s,t)$ denotes the i$^{\text{th}}$ column in the correlation matrix of session t ($t = 1, 2, 3$), subject s ($s = 1, 2.., 19$) and voxel i ($i = 1, 2, ..., 2562$) and where p,q = 1, 2, 3....,19; p $\neq$ q.

Intra-subject Variability:

$$N_i(s) = 1 - E[corr(F_i(s, t_m), F_i(s, t_n)] \tag{3.2}$$

where $m, n = 1, 2, 3$; m $\neq$ n.

$$N_i = E[N_i(s)]. \tag{3.3}$$

Inter-subject variability:

$$V_i(t) = [1 - R_i(t)] - \beta N_i - c \tag{3.4}$$

$$V_i = Mean(V_i(t)) \tag{3.5}$$

3.1.3.2 Seed Based Connectivity Analysis. To validate highly variable and less varied regions, we selected seeds from both regions in images from patient and healthy population. As a second step, the functional connectivity map indicating the seed to whole brain connectivity was computed for each individual. This map was binarized using a threshold value of 0.2. The binarized maps were averaged resulting in an estimate of percent of subjects showing a significant connectivity to the seed [77].

3.1.3.3 Bootstrap Validation. In order to determine the statistical significance of the variability differences, we applied bootstrap statistics. We randomly took 10 subjects in one iteration from both healthy and TLE groups and the inter-subject

variability was calculated after regressing out the intra-subject variance. This method was repeated 100 times. Finally, a t-test was applied on each voxel vector.

3.1.3.4 17-Network Parcellation Analysis. 17-Network parcellation scheme was perfomed based on a previously published study [78]. After the extraction of the fMRI time series data, ROIs were averaged resulting in a total of 61 ROIs for each hemisphere. The Pearson's correlation was computed between pairs of ROIs within each hemisphere. To normalize the correlation values, we applied an r-to-z transformation. As a last step, we performed an unpaired t-test in order to find the statistically significant regions between the healthy controls and the TLE patients. Results were corrected using the false discover rate (FDR) method [79]. The 17-Network parcellation ROI visualization can be observed in Figures 3.1 and 3.2.

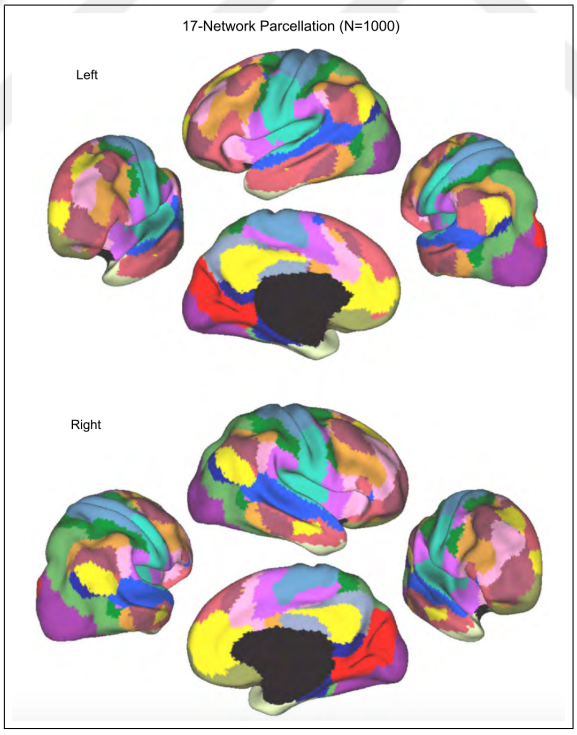

Figure 3.1 The 17-Network parcellation (Adapted from [56]).

Network (Yeo et al., 2011)	Network name (Baker et al., 2014)	Cerebral cortical regions (Yeo et al., 2011; Baker et al., 2014)	No. of voxels in eroded cerebral cortical seed	Cerebellar representation (Buckner et al., 2011)	
				Anat-omical regions	No. of voxels
N1	Visual peripheral	Striate, extrastriate	-	N/A	0
N2	Visual central	Striate, extrastriate	-	Vermis VI	14
N3	Somato-motor A	Central sulcus, secondary somatosensory	178	I-V, VIIb	489
N4	Somato-motor B	Central sulcus, secondary somatosensory, insula, auditory	356	V	241
N5	Dorsal attention A	Posterior temporal occipital, superior parietal, inferior parietal occipital	-	N/A	0
N6	Dorsal attention B	Posterior temporal, postcentral gyrus, frontal eye fields, precentral ventral frontal	67	VIIb-VIIIa	238
N7	Ventral attention	Parietal operculum, medial parietal, medial frontal, precentral ventral frontal, insula, temporal, precentral frontal, posterior temporal	117	VI, VIIIa	750
N8	Salience	Medial posterior prefrontal, ventral prefrontal, cingulate sulcus, inferior parietal, lateral prefrontal	193	VI, Crus I-II, VIIb	439
N9-10	Limbic	Temporal pole, orbitofrontal	492	White matter	1024
N11	Control C	Precuneus, posterior cingulate	-	Crus I	9
N12	Control A	Intraparietal sulcus, lateral prefrontal, posterior temporal, dorsal prefrontal, cingulate, orbitofrontal, medial posterior prefrontal, lateral posterior prefrontal	110	VI, VIIb	426
N13	Control B	Lateral posterior prefrontal, lateral anterior prefrontal, inferior parietal, temporal, medial posterior prefrontal	258	Crus I, VIIb	1154
N14	Default D (Auditory)	Temporal cortex	-	N/A	0
N15	Default C	Retrosplenial, parahippocampal complex, ventral inferior parietal	-	X	30
N16	Default A	Medial prefrontal, posterior inferior parietal, posterior cingulate, dorsal prefrontal, orbitofrontal, temporal	472	IX, Vermis IX, Crus I, Crus II	799
N17	Default B	Dorsal prefrontal, temporal, anterior inferior parietal	236	Crus I-II	1387

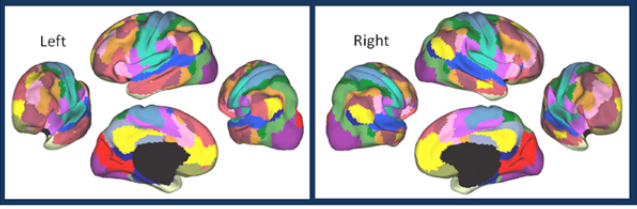

Figure 3.2 The 17-Network parcellation and their corresponding anatomical regions (Adapted from [80]).

3.1.3.5 ROI-wise Random Subspace Algorithm Analysis. In order to compute the direct relation between different brain regions, we extended the random subspace algorithm whose infrastructure was based on the seed to whole brain connectivity to seed to seed connectivity [28]. To validate the random subspace method, we generated an fMRI simulation data set based on the two-fold algorithm [81]. In the first step, given the correlation coefficients, we calculated the covariance matrix, and the pseudo-inverse of the covariance matrix. Then, we multiplied the inverse matrix with -1. To normalize the partial correlation coefficients, we divided each element dividing by the square root of the respective diagonal elements of the inverse covariance matrix (Eq. 3.6). Finally, the ground-truth partial correlation coefficients are between nodes

i and j;

$$-(\gamma_{ij})/\sqrt{\gamma_{ii}\gamma_{jj}} \tag{3.6}$$

In the second phase of the algorithm, given the covariance matrix that we generated from the correlation coefficients, we obtained n-node time series data. Based on this covariance matrix, we created an order one autoregressive model (AR(1)) with a parameter ρ=0.5 which was a sufficient lag for the preprocessed fMRI data [81] as given in Eq. 3.7:

$$y(t) = c + \rho * y(t-1) + \sigma * k \tag{3.7}$$

where c was a constant, σ=1, k is a random number with a normal distribution. After the generation of time series data, in order to evaluate the performance of the extended random subspace method for functional connectivity algorithm (E-RSMFC), we applied different partial correlation algorithms on the simulation data set. As the first solution, partial correlation method was used in Matlab® (MathWorks®, Natick, MA) environment. As a second method, the implementation inverse covariance (ICOV) with pseudoinverse solution from [82] was used. First, the covariance matrix of the generated data set was calculated. The pseudo-inverse of the covariance matrix was calculated then multiplied by -1. To normalize the partial correlation coefficients, we divided each element of multiplied pseudo-inverse covariance matrix by the square root of the respective diagonal elements of multiplied pseudo-inverse covariance matrix given in Eq. 3.6 [82]. In the last method, we determined the inverse covariance matrix using the L1 precision [83]. L1-precision solves the following optimization expression:

$$\max_{\Lambda \succ 0} \log \det\Lambda - trace(\hat{\Sigma}\Lambda) - \rho\|\Lambda\|_1 \tag{3.8}$$

where Λ=Σ^{-1}, and $\hat{\Sigma}$ is the empirical covariance matrix, $\|\Lambda\|_1$=$\sum_{ij}|\Lambda_{ij}|$ and ρ >0 denotes the penalty (regularization-controlling) parameter [83],[84]. [82] tested the parameter with different values 5, 10, 20, 50, 100, and 200. According to their findings, they have never been able to obtain best results with the values of 10, 20, 50, and 200, so they used 5 and 100 as the regularization parameter. Consequently, we used 5

as the regularization parameter for our simulation experiments. Implementation from [83] was used to find the inverse covariance matrix of the given data sets.

The detailed summary of the extended random subspace method for functional connectivity algorithm (E-RSMFC) is given as follows:

Input: time series data for p ROIs

Output: partial correlation coefficients for p ROIs

Step 1:

(1) Randomly shuffle the regions by storing the original indices

(2) Take first maximum number of p_1 ROIs and concatenate them to the end of the shuffled matrix whose voxel size is p

(3) To calculate the covariance and inverse covariance matrix, divide this permuted matrix into sub-matrices such that each submatrix has number of p_0 ROIs.

Step 2:

(1) Calculate covariance matrices.

(2) Take the pseudo-inverse of each submatrix.

(3) Compute partial correlation coefficients for each subset.

(4) Calculate the mean of partial correlation coefficients that are computed in each iteration.

(5) Compute steps 1-2 t times till the result converge to a minimum error.

Mainly, two critical tuning parameters need to be adjusted in order to get the optimum solution of the algorithm. The number of ROIs in each subspace (p_0) and the number of concatenated ROIs (p_1). To do so, we iteratively computed partial correlations starting from 10 node and increased the number of nodes to 50. After 50 nodes trial, we applied the algorithm on data sets having 60, 70, 80, 90, 122 nodes separately. Thus, to test the algorithm, we created 20 data sets for all nodes. Starting from 10 node data set, we iteratively tried the algorithm for different subsets by adding maximum number of nodes to the end of each data set (p_1). As a result each subset

has p_0 ROIs in it, and all ROIs appeared in each subset once, Eq. 3.9.

$$(p + p_1)/2 = p_0 \tag{3.9}$$

As the last step of the partial correlation estimation, we performed statistical analysis to confirm the statistical significance of the estimated partial correlation coefficients compared to other methods. To do so, we applied F-test on the coefficient of determination values. To assess the estimation accuracy of the random subspace algorithm, for 20 data set, the average normalized mean square error, coefficient of determination were calculated for 10, 50, 60, 70, 80, 90, 122 nodes on the simulation data for 120 time points. The normalized mean squared error (NMSE) was computed based on the following formula:

$$MSE = \frac{\Sigma_{i=1}^{n}(X_{obs,i} - X_{model,i})^2}{n} \tag{3.10}$$

$$NMSE = \frac{MSE}{X_{obs,max} - X_{obs,min}} \tag{3.11}$$

where X_{obs} = the values actually observed from the environment that is being modeled, X_{model} = values predicted by the model [85],[86]. The coefficient of determination was calculated as follows [87]:

$$R^2 = 1 - \frac{SS_{RES}}{SS_{TOT}} = 1 - \frac{\Sigma_{i=1}^{n}(Y_{obs,i} - Y_{model,i})^2}{\Sigma_{i=1}^{n}(Y_{obs,i} - \overline{Y_{obs}})^2} \tag{3.12}$$

where Y_{obs} = the values actually observed from the environment that is being modeled, Y_{model} = values predicted by the model

R^2 indicates the "goodness-of-fit " of a model fitted to the data [87]. If the coefficient of determination value is close to 1, this implies a good fit to a model.

4. RESULTS

In this chapter, the inter-subject variability results together with the 17-Network parcellation results are shown as well as the extended random subspace algorithm and its application on both the TLE patients and healthy controls fMRI data.

4.1 Inter-subject Variability Results

The inter-subject variability results revealed that the TLE patients showed a greater variability in the frontoparietal control, the ventral/dorsal attention, the default mode, the somatomotor, the visual and limbic resting state networks compared to controls based on the 7-network parcellation [56]. The inter-subject variability map is given in Figure 4.1. In order to recognize the functional variability difference between healthy controls and patients with temporal lobe epilepsy, we subtracted intra-subject regressed inter-subject variability map of controls from patients. The difference map together with the clustering validity index is given in Figure 4.2.

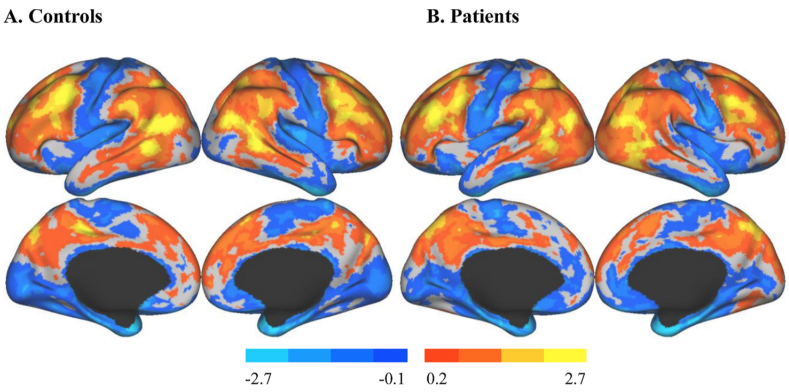

Figure 4.1 Intra-subject regressed inter-subject variability results (A) Controls (B) Patients.

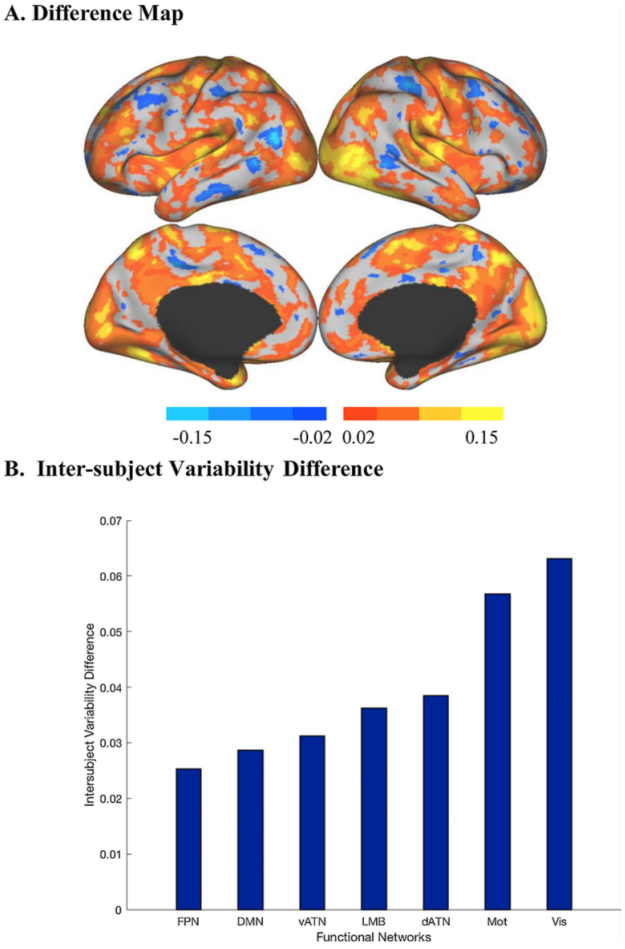

Figure 4.2 (A) Average inter-subject variability differences in resting functional connectivity between patient and healthy populations (TLE > Healthy). Yellow regions show highly varied, dark blue regions show less varied anatomical regions between two populations. (B) Average inter-subject variability difference quantified based on the difference map (A) and the 7-Network parcellation [56]. FPN indicates frontoparietal control; DMN default mode; vATN ventral attention; LMB limbic; dATN dorsal attention; Mot sensory-motor and Vis visual networks.

The high and less varied regions were also confirmed by selecting a highly and less varied seeds and the seed to whole brain connectivity was computed for both healthy and patient groups. The results were also in favor of the argument that TLE patients presented a higher variability when a highly varied seed was to be selected and less variability when a less varied seed was to be. The results are given in Figures

4.3 and 4.4.

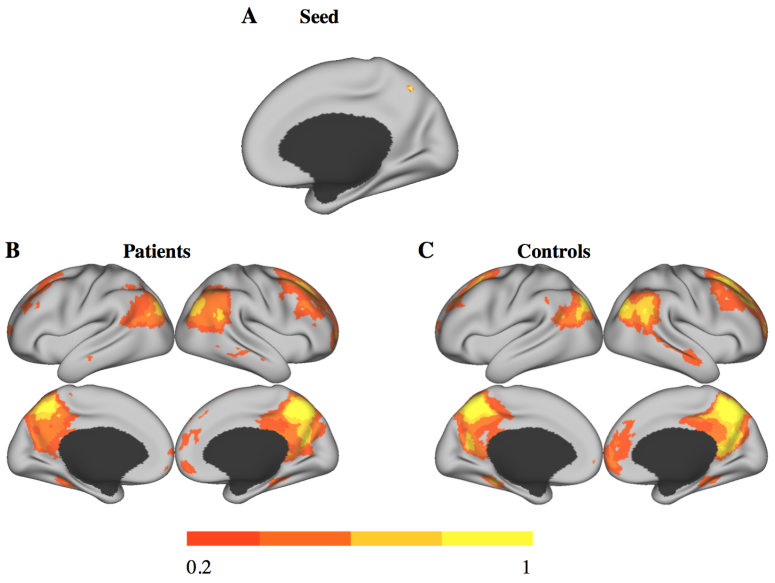

Figure 4.3 (A) Highly varying seed on the right hemisphere for the (B) TLE population and (C) Healthy population.

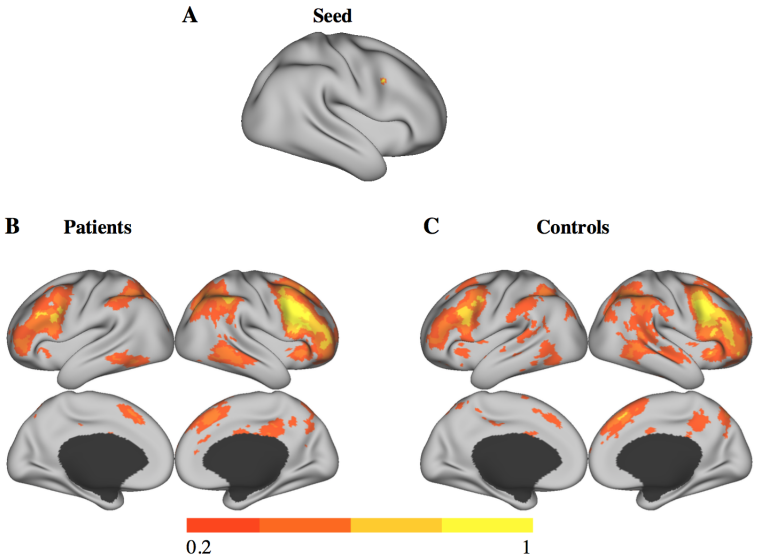

Figure 4.4 (A) Less varying seed on the right hemisphere for the (B) TLE population and (C) Healthy population.

The results were further analysed with the bootstraping method in order to

validate the statistical significance of the difference map. According to bootstrap results based on the intra-subject regressed inter-subject variability, the variability in frontoparietal, somatomotor, ventral/dorsal attention, default mode, visual and limbic resting state networks was statistically significant between patient population and healthy controls shown in Figure 4.5 ($p<0.05$) based on the 7-network parcellation [56]. Thus, the results confirmed that the TLE patients showed higher variability on the same networks with the difference map.

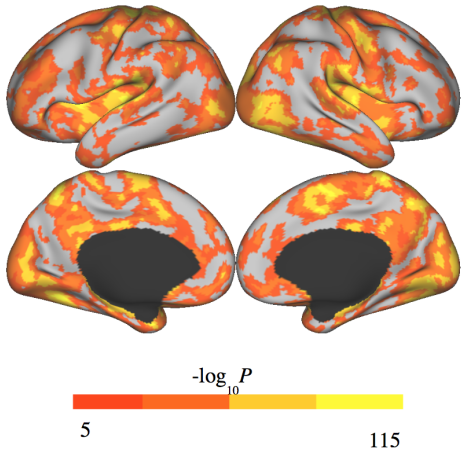

(a)

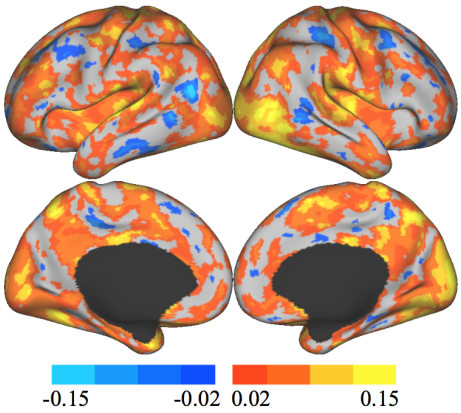

(b)

Figure 4.5 (a) Bootstrap t-test results statistics for -$\log_{10} P$ (b) The difference map, $TLE>Healthy$.

4.2 17-Network Parcellation Results

The functional connectivity maps that belong to each group were obtained by computing the Pearson's correlation matrices using 17-Network parcellation [78]. From 3721 region comparisons, 66 ROIs were found to be statistically significant between inter-hemispheric ROIs ($q < 0.05$, FDR-corrected). Thereby, there were substantial differences in functional connectivity patterns between patient and healthy groups. Hence, functional connectivity mostly decreased in between and within the networks frontoparietal control, the default mode, the ventral attention, the visual, the somatomotor, the saliency and the dorsal attention in patient population as shown in the average Pearson correlation matrices for each group in Figure 4.6. In the TLE patients, inter-hemispheric functional connectivity results demonstrated a signicant negative increase (FDR-corrected, $q < 0.05$) in connectivity between the somatomotor cortex and lateral prefrontal cortex. Statistical results are given in Manhattan plot in Figure 4.7. The TLE patients also showed significant positively increased functional connectivity between the left and the right hemisphere pairs of ventral attention and dorsal attention. Additionally, the region-wise statistical results were given in Figure 4.8 and Figure 4.9.

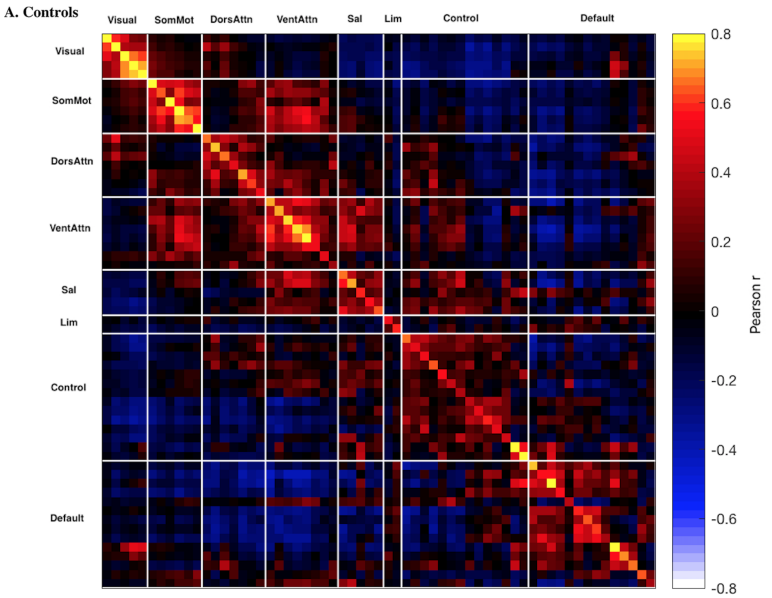

(a)

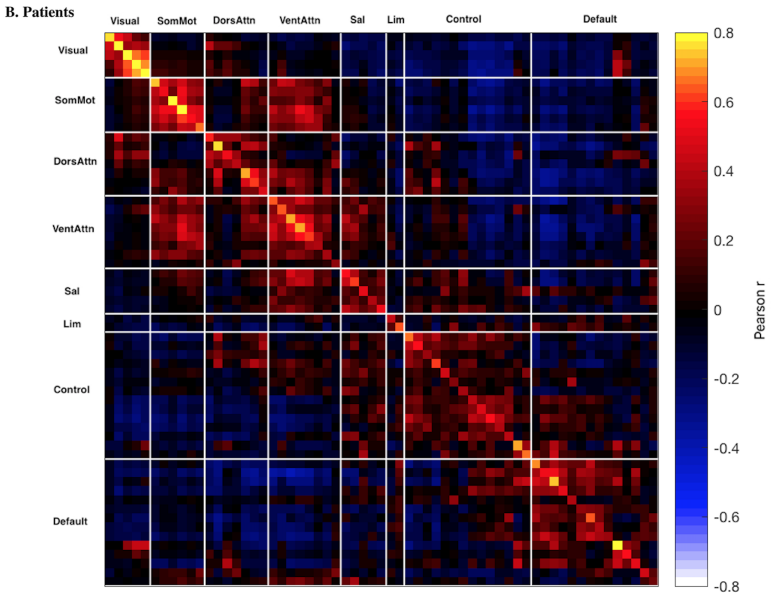

(b)

Figure 4.6 Each grid shows inter-hemispheric functional connectivity correlation matrices for ROIs (based on Pearson correlation(r)) in Controls (A) and Patients (B). SomMot indicates somatomotor, DorsAttn, dorsal attention, VentAttn, ventral attention, Sal, saliency, Lim, limbic.

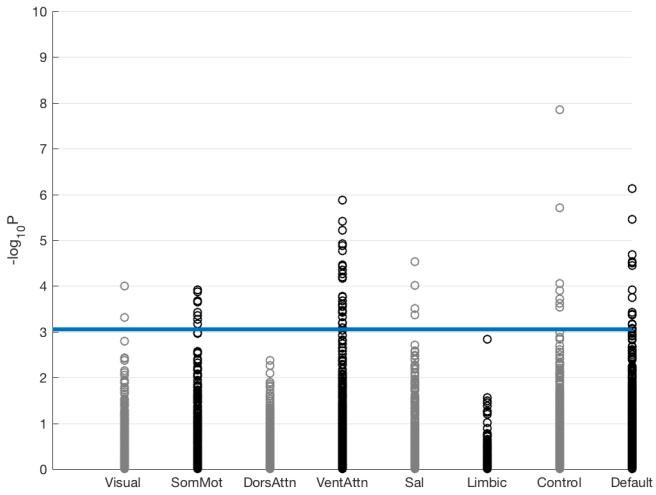

Figure 4.7 Manhattan plot for p values between left and right hemisphere between network functional connectivity differences. The y-axis shows the -$\log_{10} p$ values of 3721 between-network regional pairs, and the x-axis shows their corresponding anatomical positions. The horizontal blue line represents the threshold of $p = 8.86 \times 10^{-4}$ that corresponds to the false discovery rate ($q < 0.05$) (Note: Each between network connection is plotted twice to reflect both regions.).

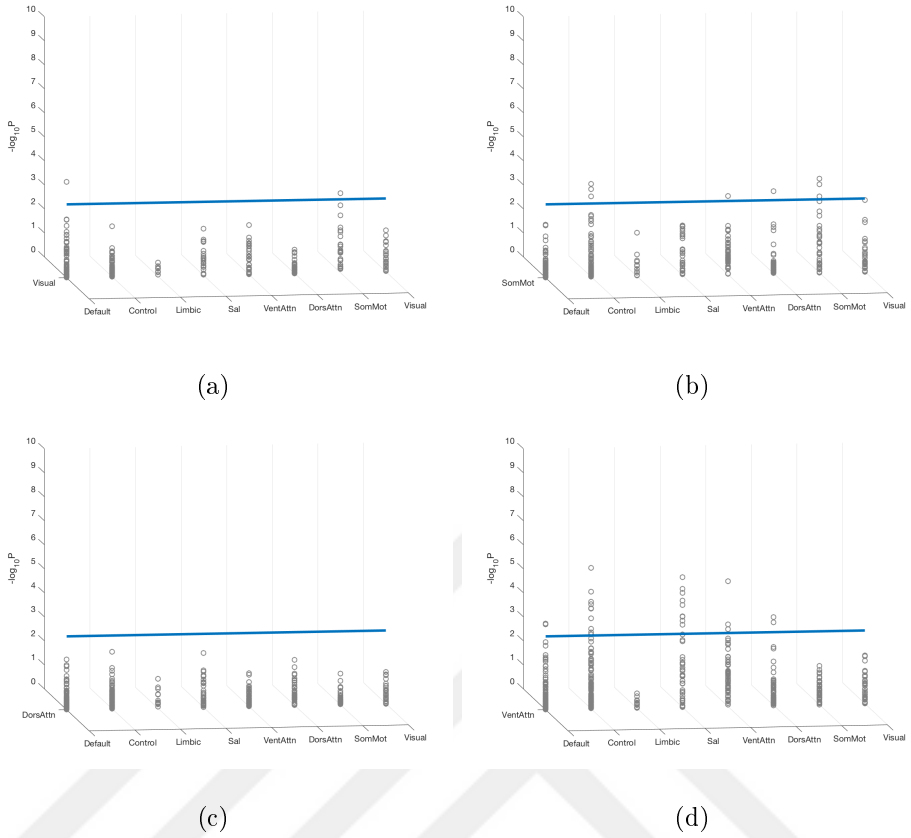

(a) (b)

(c) (d)

Figure 4.8 Region-wise manhattan plot for p values between left and right hemisphere between network functional connectivity differences. The horizontal blue line represents the threshold of $p = 8.86 \times 10^{-4}$ that corresponds to the false discovery rate ($q < 0.05$).

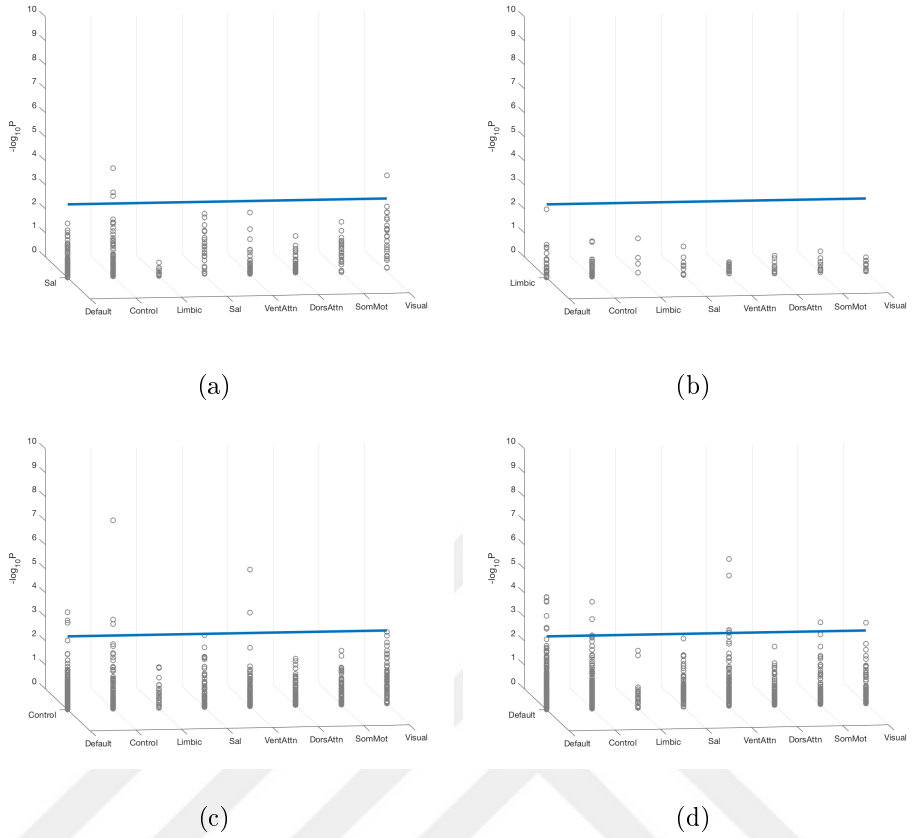

(a) (b)

(c) (d)

Figure 4.9 Region-wise manhattan plot for p values between left and right hemisphere between network functional connectivity differences. The horizontal blue line represents the threshold of $p = 8.86 \times 10^{-4}$ that corresponds to the false discovery rate ($q < 0.05$).

The functional relation between dorsal attention, frontoparietal control and default mode networks can also be observed in Figure 4.10. According to the spring graph, the network clusters belonging to the patient group represent more dispersed maps compared to those of the controls with an implication of decreased functional connectivity patterns in the patient population.

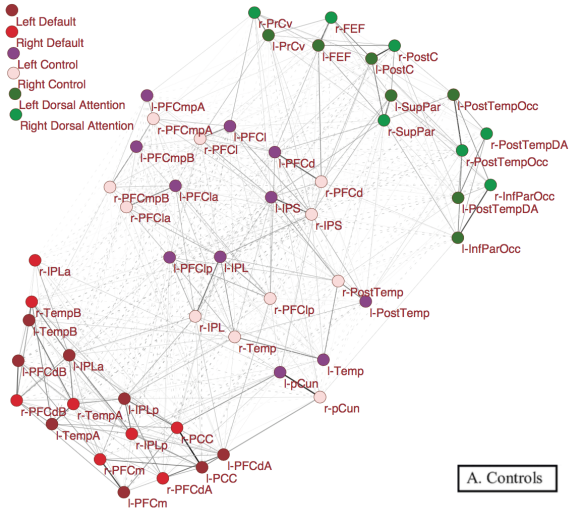

(a)

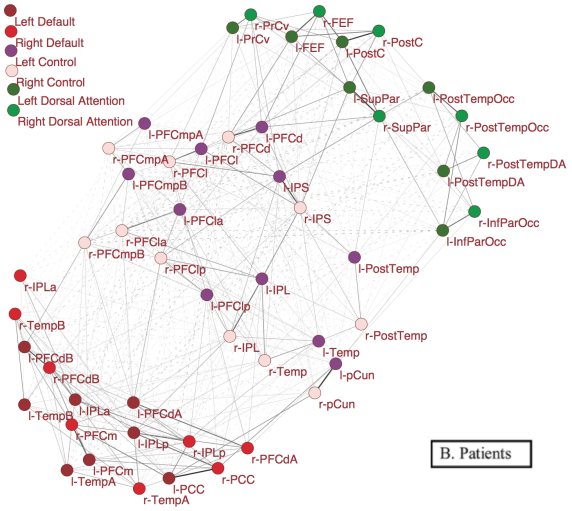

(b)

Figure 4.10 Spring-loaded graphs demonstrating the bilateral hemispheric anatomical regions (a-b), for dorsal attention, default mode and frontoparietal control networks, (a) Healthy controls (b) TLE (Abbreviations for the anatomical regions from [78] can be found in Appendix B).

4.3 ROI-wise Random Subspace Algorithm Results

We iteratively ran the algorithm given in Subsection 3.1.3.5 for all the data sets so as to find the optimal parameters that yielded the minimum error between the estimated and ground-truth matrices. To validate the algorithm, we first applied it on 10-node data set with 120 time points. For this dataset the parameters were selected as $p_0 = 10$, $p_1 = 10$; $p_0 = 9$, $p_1 = 8$; $p_0 = 7$, $p_1 = 4$; $p_0 = 8$, $p_1 = 6$; $p_0 = 6$, $p_1 = 2$; $p_0 = 5$, $p_1 = 10$; $p_0 = 4$, $p_1 = 10$. As p_0 and p_1 values becomes lower, the estimated partial correlation values diverged from the ground-truth matrices. In other words, the ANMSE increased and the AR^2 values decreased. For the partition $p_0 = 10$, $p_1 = 10$, the E-RSMFC algorithm is equivalent to the other methods in performance ANMSE and AR^2. Hence, this finding clearly proves the reliability of the algorithm implementation. Considering the effect of p_0 on the inverse covariance matrix calculation, we found that, as the number of regions inside submatrix decreased, the correctness of the partial correlations diverged from the the ground-truth matrices (Figure 4.11). As the data set dimension increased the inverse of covariance matrix became unstable, implying a divergence from the ground-truth. In order to test this fact, we also applied the E-RSMFC algorithm on 50, 60, 70, 80, 90 and 122 nodes data sets with various p_0 and p_1 values. The error became larger when the number of regions increased, i.e. when the average normalized mean squared error ≥ 0.01, this algorithm gives accurate results when dimension is less than 90 for 120 time points. The average normalized mean square error and the average coefficient of determination results of the algorithm is given for the optimal partitions in Figure 4.12.

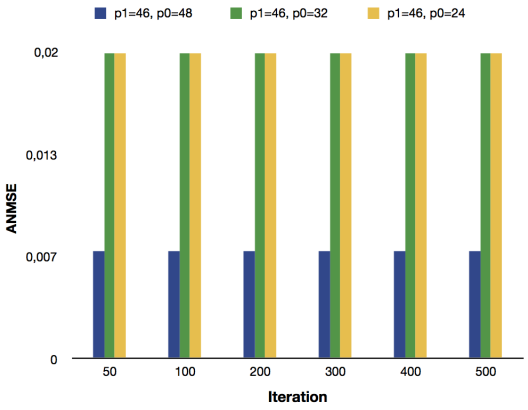

(a)

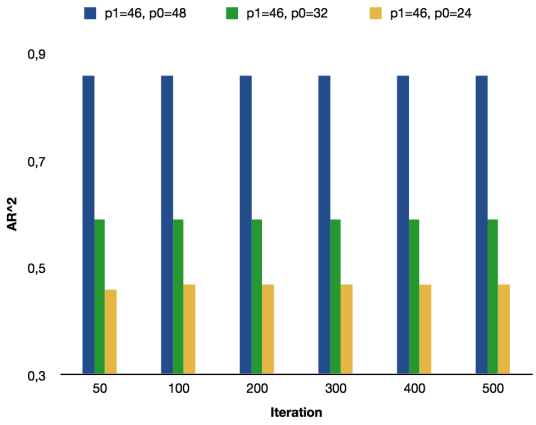

(b)

Figure 4.11 (a) The average normalized mean squared error and (b) The average coefficient of determination comparison for different p_0 values, $p_1 = 46$ for the 50 node data set.

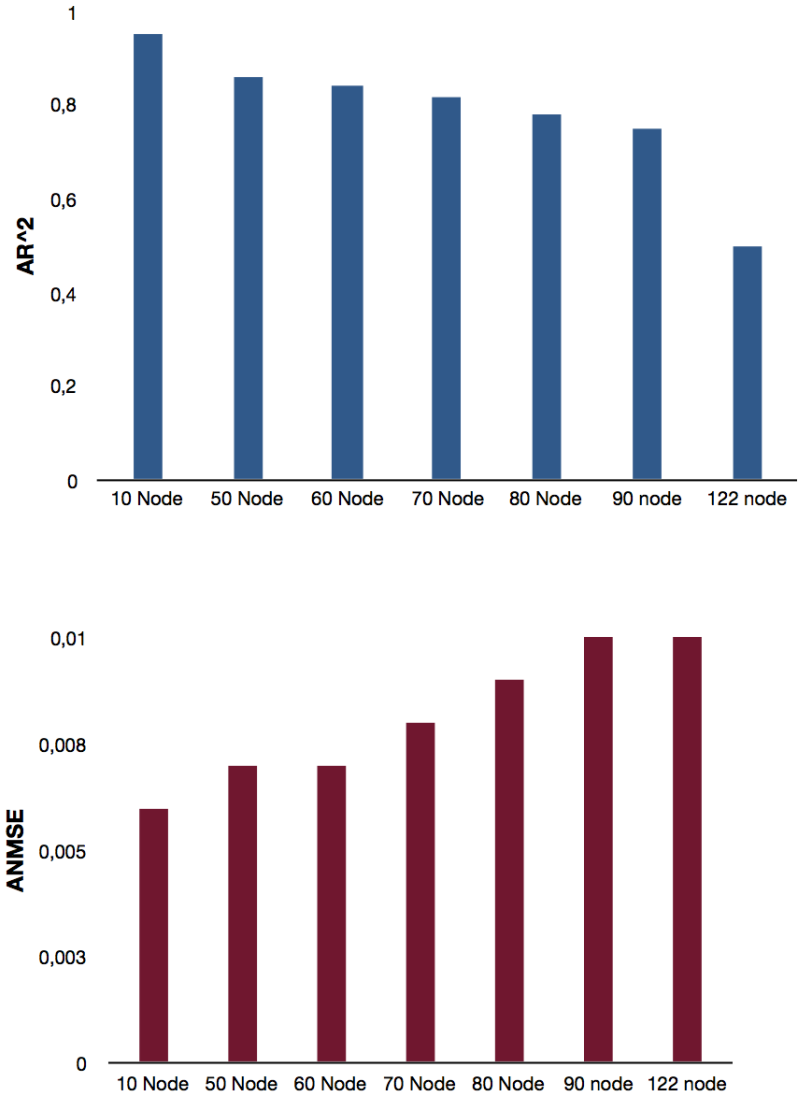

Figure 4.12 The average coefficient of determination (AR^2) and the average normalized mean square error (ANMSE) for the E-RSMFC algorithm.

Iteration number was also another issue to consider while running the algorithm. Hence, after 50 iterations the algorithm became stable, so in order to ensure stability, we chose 100 as the maximum iteration number for each data set. The performance evaluation summary for the optimal algorithm parameters is given in Figure 4.13.

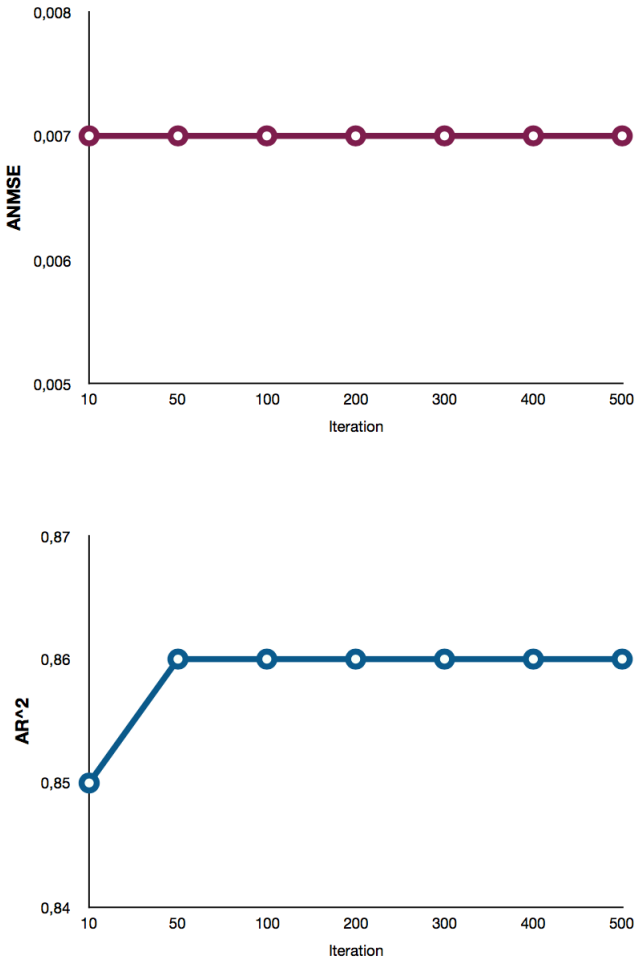

Figure 4.13 The average normalized mean square error (ANMSE) and the average coefficient of determination (AR^2) changes according to iteration for the 50 node data set.

After having the optimal parameters for the E-RSMFC, we compared the E-RSMFC with pseudoinverse inverse covariance (ICOV-P), Matlab partial correlation solution (MPC) and L1 shooting algorithm (L1) with the regularization parameter $\lambda = 5$. We chose the regularization parameter $\lambda = 5$, since [82] noted the best results obtained when $\lambda = 5$. Results revealed that as the number of number of regions (p) approach to number of time points (n); E-RSMFC algorithm outperforms the other three methods by having a lower mean squared error as well as higher mean coefficient of determination values. Finally, we used F-test to compare the statistical significance

of different methods according to their coefficient of determination values. According to results, there is no statistical significance in predicting ground-truth covariance matrices between MPC and E-RSMFC (p=0.49), ICOV-P and E-RSMFC (p=0.49) and L1 and E-RSMFC (p=0.63) for the 10-node data set. In the case of 50 node data set, there is statistical significance between E-RSMFC, MPC (p=0.03), ICOV-P (p=0.03) methods and there is no statistical significance when comparing with L1 (p=0.06) method when estimating the ground truth covariance matrices. For the 60 node data set, according to F test results, there is a statistical significance between MPC and E-RSMFC (p=0.007), ICOV-P and E-RSMFC (p=0.007) and L1 and E-RSMFC ($p = 1.03 \times 10^{-12}$) when estimating the ground-truths. As for the 70 node data set, according to F test results, there is statistical significance between MPC and E-RSMFC (p=0.03), ICOV-P and E-RSMFC (p=0.03) and L1 and E-RSMFC ($p = 2.08 \times 10^{-14}$) when estimating ground truth covariance matrices. Lastly, for the 80 node data set, according to F test results, there is a statistical significance between MPC and E-RSMFC ($p = 8.36 \times 10^{-8}$), ICOV-P and E-RSMFC ($p = 8.36 \times 10^{-8}$) and L1 and E-RSMFC ($p = 0$) when estimating the ground truth covariance matrices. The method comparisons are given in Figure 4.14. To sum up, the random subspace algorithm outperforms other existing methods in terms of accurately computing the inverse covariance and partial correlation coefficients for 50, 60, 70, 80 nodes as well as showing statistical significance for the 50, 60, 70 and 80 number of nodes with 120 time points.

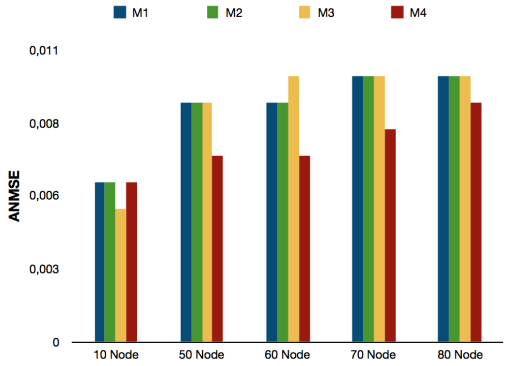

(a)

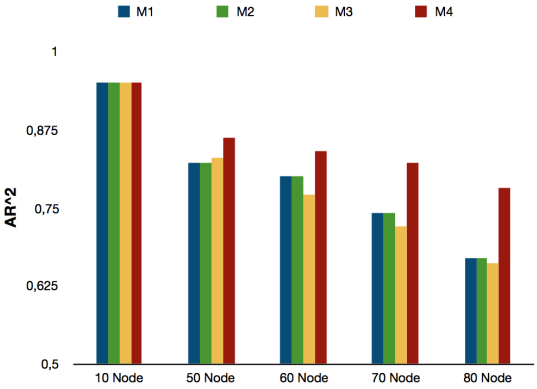

(b)

Figure 4.14 (a) The average normalized mean squared error and (b) The average coefficient of determination comparison for different methods, M1: Inverse covariance (ICOV) with pseudoinverse, M2: Matlab partial correlation solution, M3: L1 Shooting partial correlation with the regularization parameter $\lambda = 5$, M4: Random subspace algorithm results on 10, 50, 60, 70 and 80 node data sets.

4.4 E-RSMFC Application to Healthy Population and Temporal Lobe Epilepsy Patients' Resting State fMRI Data

We used a 17- network parcellation framework which was previously published in [78]. Aforementioned in literature, TLE patients exhibited deterioration in dor-

sal/ventral attention, default mode and frontoparietal control resting state networks [34],[46],[88],[89],[90]. Thus, we chose 80 ROIs (with the optimal parameters $p_0 = 76$, $p_1 = 72$) from 122 ROIs including dorsal/ventral attention, default mode and frontoparietal control resting state networks. Among 80 ROIs, patients with TLE mostly showed a decreased functional connectivity using both partial correlation and Pearson correlation coefficients. According to partial correlation results, 120 ROIs including the dorsal/ventral attention, the frontoparietal control, the default mode, had statistically significant differences between healthy population and TLE patients ($p<0.05$, uncorrected). There were no statistically significant results when correction was performed. However, 45 ROIs including ventral/dorsal attention, frontoparietal control, default mode, revealed statistically significant results between healthy and patient population using Pearson correlation (FDR-corrected, $p=0.0014$). Both Pearson and partial correlation results for bilateral structures are given in Figures 4.15 and 4.16 for healthy and patient populations. As it is known that homotopic structures are connected with each other after regressing out the effect of other brain regions [68],[91], we only presented the homologous structures in this framework.

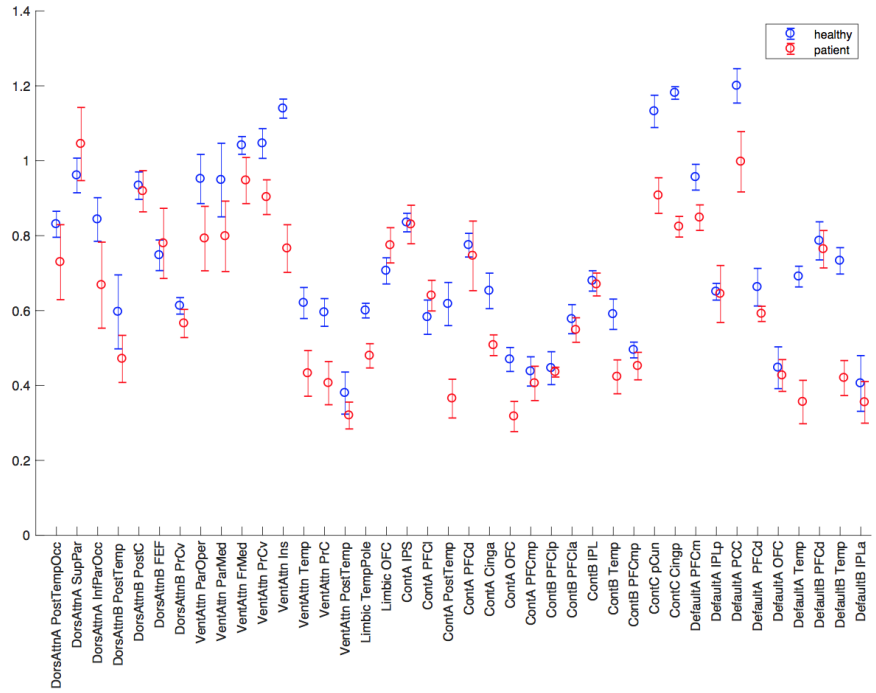

Figure 4.15 The error bars representing the z-value of the Pearson correlation coefficients for both healthy and patient group (Anatomical region abbreviations can be seen in Figure 3.2).

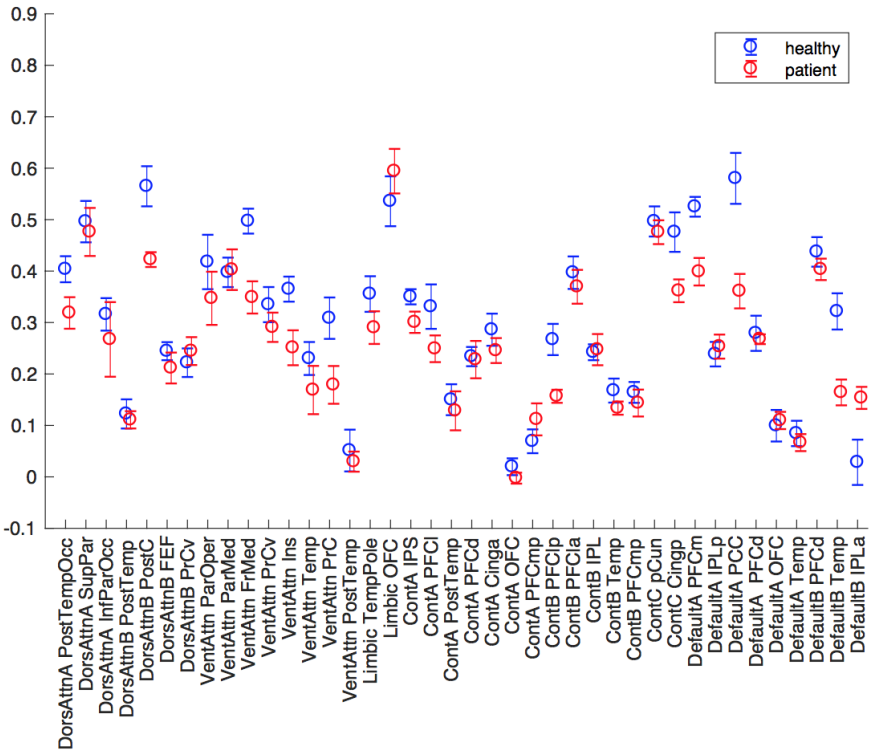

Figure 4.16 The error bars representing the z-value of the partial correlation coefficients for both healthy and patient group (Anatomical region abbreviations can be seen in Figure 3.2).

5. DISCUSSION AND CONCLUSION

In this work, we investigated the functional inter-subject variability and connectivity in order to assess the effect of temporal lobe epilepsy on resting-state brain networks by comparing the resting state fMRI scans of TLE patients with those of the healthy population. To accomplish this framework, we made use of both Pearson's and partial correlation coefficients. We have reached several substantial conclusions about functional inter-subject variability and connectivity. According to our functional inter-subject variability results, TLE patients exhibit higher variability in the default mode network in the areas as the PCC/Precuneus, the anterior cingulate (ACC), the medial prefrontal cortex; the frontoparietal control network including the dorsolateral prefrontal cortex, the orbitofrontal cortex; the dorsal attention network including the frontal eye fields, and the ventral attention network including the temporoparietal junction, the insula, the somatomotor network including the motor region, the visual and the limbic networks, can be observed from the Figures 4.1 and 4.2. TLE has been shown to be a prevalent network disease [23],[88],[89],[90]. Hence, there has been no compromise related to the deteriorated networks because of the fact that same patient having a single clinical expression may show different seizure propagation pathways [92]. Beyond this, it has been noted that TLE has a unique functional connectivity patterns although two different patients may have a similar seizure onset zones on the temporal region which is shown by the intracranial EEG [44]. Stemming from variable seizure onset localization and morphological measures in patients, TLE has been considered as a heterogeneous disease [92],[93],[94],[95]. In summary, at the single subject level, there is variability in the functional connectivity patterns within the same epileptic patient population [44],[96]. The seizure onset is thought to be located in hippocampus or parahippocampal gyrus in TLE [34]. DMN BOLD activity increases in case of an internal attentional engagement, e.g. remembering past events or envisioning the future [97] and the posterior cingulate is one of the core anatomic structure that belongs to the DMN [35]. Considering this fact, DMN is one of the core disrupted networks effecting the functional connectivity in the TLE patient population [34],[52],[53],[98].

For instance, [98] have shown a significant functional connectivity difference between the DMN and the executive control network when they compared those TLE patients having normal (G1) and those having impaired executive functioning (G2) with the healthy population using the resting state fMRI. The normal G1 and the healthy group had no significant negative functional connectivity. On the other hand, the G2 had a significantly enhanced negative correlation with respect to the healthy controls and the G1. They explained this fact as a decreased interaction between the mPFC (medial prefrontal cortex) and the dlPFC (dorsolateral prefrontal cortex) considering that these belonged the core hubs of default mode and executive control networks. Besides that, [99] have found a positively correlated functional connectivity between the dorsal DMN and executive control network. At this point, it is worth to compare our results with the afermentioned studies. According to our results, the functional connectivity between the left mPFC and the right lateral prefrontal cortex (including dlPFC) is decreased in the TLE patients when compared to the healthy population ($p=0.03$, uncorrected). We also found a decrease between bilateral sensorimotor structures which was also illustrated in the previous studies [46],[88]. According to another study, however, an increased functional connectivity has been noted in the sensorimotor network [90]. Besides, [88] reported an increased functional connectivity within primary visual cortex as well as an attenuation between bilateral MT+ (a higher order visual cortex) areas of the visual network in bilateral TLE patients. Considering the fact that we found a high functional variability in the visual cortex, the results in [88] also support our findings. Our inter-subject variability results elucidate a high dissimilarity within the somatosensory and default mode networks in TLE patients compared to controls (Figure 4.2). This may pave the way to clarify the equivocal results presented in some previous studies. Besides these networks, hypo- and hyper-connectivity results revealed in former studies [23],[46],[89],[100] also support our high variability findings in the frontoparietal control and the ventral/dorsal attention networks. Each patient may have a different seizure propagation pathway. Therefore, the heterogeneity may be stemming from the discrepancy of the affected networks. In other words, some regions may be disrupted in some patients, whereas they may stay intact in others [101]. In our study, we mostly found a decreased functional connectivity between/within the networks that were less differently varied (frontoparietal control, default mode and

ventral attention) between TLE patients and controls based on the 17-Network parcellation. As a result, this prominent finding may imply that these networks are severely deteriorated in patients with TLE.

From a clinical aspect, seizures still occur in 10−40% of the TLE patients in the postoperative phase [102]. In their study, 36% of the patients MRIs were considered as normal although they had hippocampal sclerosis on their pathology. Given this complication, it is noteworhty to clarify the variability in order to define a robust biomarker related to the disease. Thereby, according to our functional variability results, less varied seeds between patient and healthy population may be used to identify a common connectivity structure which discriminates the TLE patients from the healthy population.

We further explored the functional connectivity between the healthy and patient populations based on the 17-network parcellation scheme [78]. In the concept of functional connectivity, a hypoconnectivity refers to a cognitive impairment within or between networks, whereas a hyperconnectivity may indicate a compensatory mechanism that fulfills the function loss [89]. In line with the previously published results [22],[24],[46],[88],[89],[103], our functional connectivity results revealed a significant reduction in the patients group including the frontoparietal, the somatomotor, the default mode, the ventral/dorsal attention, the saliency and the visual network. Although partial correlation results were not statistically significant when corrected, bilateral homologous structure results also supported the attenuation in the functional connectivity. This inter-hemispheric connectivity results revealed a disrupted synchronization between the hemispheres as indicated in the previous research [104].

The frontoparietal control network is functionally associated with the attention, problem solving, decision making and reasoning including lateral prefrontal cortex, anterior cingulate cortex, and inferior parietal lobule [105],[106]. It has been hypothesized that it regulates the information that are related to dorsal attention and default mode networks as well as sustaining the dynamic balance between these networks [78],[97],[107]. As one of the main regions residing within the frontoparietal control

network, the Precuneus, connects the default mode and the dorsal attention networks [107]. The Precuneus is functionally thought to associated with cognitive functioning, attention, episodic memory, mental imagery (such as motor imagery), consciousness and self-consciousness [108],[109],[36]. According to a study, there was a reduced functional connectivity between the hippocampus and the precuneus in mTLE patients [110]. In light of these, the results of our study showed that there was a reduction in the functional connectivity between the left precuneus and the right posterior cingulate, and between the bilateral posterior cingulate in patients with the TLE. According to a SPECT study, there was an ictal hypoperfusion in the superior frontal gyrus and the precuneus in 90% of the TLE patients. In another study using video EEG and SPECT, a focal decrease in cerebral blood flow (CBF) in the DMN regions such as the posterior cingulate cortex/precuneus, the inferior parietal lobule, and the medial frontal/anterior cingulate cortex, as well as in the orbital frontal, and the inferior lateral frontal cortex during complex partial seizures with decreased consciousness was observed whereas these changes were not existing in patients with preserved consciousness during simple partial seizures [109]. According to another study, the cognitive impairment of a patient may be estimated from the connectivity between posterior cingulate cortex (PCC) and left hippocampus. The results reveal that the left temporal lobe epilepsy patients who have higher connectivity between posterior cingulate cortex and left hippocampus (HC) have greater memory decline after the resection of left temporal lobe in the post surgical phase, whereas if there is higher connectivity between the PCC and contralateral HC, this do not cause any memory decline or cause less memory decline [52]. In our study, as well as a deterioration between precuneus and posterior cingulate and the bilateral posterior cingulate, there was a disruption in connectivity between the default mode network and the frontopariatel control/the ventral attention/the default mode networks implies a certain breakdown in the frontoparietal and the default mode networks suggesting an impaired consciousness in the TLE patients. This finding was also supported by the inter-subject variability results which indicated that these networks were determined as less differently varied between patient and healthy population.

Attention network is composed of ventral and dorsal attention. Ventral attention

(VA) is associated with the bottom up attention mechanism which is driven by a salient sensory input. Dorsal attention (DA) which is also called a top down attention is related to a past experience rather than sensory stimuli [111],[112]. According to a study, there was a reduction in P300 amplitude in temporal and frontal regions with an implication ventral fronto-temporo-parietal attention system impairment in the TLE patients. It has been hypothesized that the deterioration in attention network in the TLE patients is caused by the ventral network′s temporal node. Our results shed light on this argument that there is a significant decrease between the ventral attention temporal lobe and the saliency/the default mode/the ventral attention/the frontoparietal control and the dorsal attention networks.

We have proposed and implemented an extended random subspace algorithm based on the random matrix theory [74]. As Hoyle [74] stated in their work, we utilized from the computation of the inverse of the small covariance matrices to better approximate the large covariance matrix, thus partial correlations. Therefore, we have validated its high accuracy by having a minimal means square error and high coefficient of determination values on the average when compared to MPC, ICOV-P and L1 methods. It has been noted that given number of regions k and number of time points N, it is suitable to compute partial correlations when N>2k for fMRI connectivity analysis [113]. We found that when N=120 and k=60,70,80, E-RSMFC gives statistically significant results in coefficient of determination compared to all other methods. So as the number regions converges to 2k, the estimation of partial correlations becomes unstable due to dimensionality problem. In this context, for our algorithm there are two parameters that effect the accuracy of the algorithm. First one is the number of regions in each sub-matrix (p_0), and the second is the number of regions juxtaposed to the end of the regions (p_1). As a result, although the number of appended regions is critical to estimate the partial correlation coefficients with a minimum error rate, the number of regions within the subgroup should be adjusted according to a k/N ratio. p_1 should be the maximum number of nodes that could be appended to the end by keeping the k/N ratio minimum in each submatrix in order to make a better approximation.

The partial correlations related to the bilateral homologous structures were con-

firmed by having strong functional connections as previously stated in [26],[68] for the healthy population. Since it has been shown that brain has a stronger between homotopic functional connectivity compared to that of between heterotopic regions due to the structural connectivity via corpus callosum (CC) [91]. The bilateral homologous structures belonging to dorsal attention, ventral attention, frontopariatel control and default mode networks were found to be attenuated in patient population ($p<0.05$) corroborating the previously disrupted networks found using the Pearson's corelation coefficient.

Anatomically connected regions are also functionally correlated, in contrary to the functionally correlated regions which do not necessarily be structurally connected [69]. It has been hypothesized that partial correlations may also give an idea about the structural connectivity between regions [68],[114]. According to a previously published research, there was a reduction in structural connectivity between bilateral posterior cingulate regions in patients with TLE [115]. We found a decrease in functional connectivity between bilateral posterior cingulate regions using both correlation and partial correlations ($p<0.05$). Besides, DeSalvo et al. [116] examined the structural connectivity in the left TLE patients and found that between-module connectivity decreased in the bilateral lateral frontal, the inferior parietal, the medial orbitofrontal, and the temporal cortices. In particular, the structural connectivity was decreased in the DMN assessed by both within and between-module connectivity. This finding also supports our results that the decreased functional connectivity within the DMN including the bilateral temporal cortices in both correlation (FDR-corrected) and partial correlation results ($p<0.05$, uncorrected) suggest white and gray matter degeneration in the TLE patients. Although these results need to be confirmed with an fMRI/DTI study, we may infer that the partial corelation has a close relationship with both structure and function.

A decrease accompanied with a high variance in functional connectivity mainly among the default mode, the frontoparietal, the ventral attention, the dorsal attention and the somatomotor networks may play an important role in identifying the disease pathology in terms of large scale functionally impaired networks. As a result, all these

findings shed light on the hypothesis that the disrupted large-scale networks are not only restricted to an impairment in the temporal lobe but also pointing out to some significant effects in other brain regions [110],[116].

5.1 Limitations of the study:

This study has several limitations including the small sample size of patients with the TLE together with their clinical characteristics. The data from the patients regarding seizure frequency, epilepsy duration and antiepileptic drugs were unfortunately unavailable. As for the E-RSMFC algorithm, so as the error becomes larger when the number of regions increases, only when the average normalized mean squared error>0.01, this algorithm gives accurate results when the dimension is less than 90 for 120 time points.

5.2 Future Work

In future, the effect of factors such as seizure frequency, epilepsy duration and antiepileptic drugs together with laterality and gender may be included as confounding factors to assess the inter-subject variability and functional connectivity in TLE. In E-RSMFC, partial correlation estimation may be computed via the L1- and the L2-norm regularizations or with their combinations in order to have a better approximation.

5.3 List of publications produced from the thesis

1. Investigation of functional variability and connectivity in temporal lobe epilepsy: A resting state fMRI Study, S. N. Dumlu, A. Ademoğlu, W. Sun, "*Neuroscience Letters*, Vol. 733, pp. 135076, 2020.

APPENDIX A. DEMOGRAPHIC INFORMATION

Table A.1 The demographic data of 19 TLE patients.

Number	Gender	Age
1	f	47
2	m	38
3	f	26
4	f	26
5	f	25
6	f	23
7	m	20
8	f	14
9	f	19
10	m	25
11	f	27
12	f	52
13	m	25
14	m	48
15	f	21
16	f	16
17	f	31
18	m	41
19	f	17

Table A.2 The demographic data of 19 healthy controls.

Number	Gender	Age
1	m	20
2	m	23
3	m	25
4	m	25
5	m	37
6	m	40
7	f	20
8	f	21
9	f	21
10	f	21
11	f	22
12	f	23
13	f	23
14	f	23
15	f	23
16	f	24
17	f	25
18	f	28
19	f	29

APPENDIX B. ANATOMICAL REGION ABBREVIATIONS

FEF, frontal eye fields,

InfParOcc, inferior parieto-occipital,

IPLa, lateral inferior parietal lobule,

IPLp, posterior inferior parietal lobule,

PCC, posterior cingulate,

pCUN, precuneus,

PFCdA, dorsal anterior prefrontal cortex,

PFCdB, B component of dorsal prefrontal cortex,

PFCl, lateral prefrontal cortex,

PFCm, medial prefrontal cortex,

PFCmpA, A component of medial posterior prefrontal cortex,

PFCmpB, B component of medial posterior prefrontal cortex,

PostC, postcentral gyrus,

PostTempOcc, posterior temporal occipital,

PrCv, ventral precentral gyrus,

SupPar, superior parietal lobule,

Temp, temporal cortex,

TempA, A component of temporal cortex,

TempB, B component of temporal cortex.

REFERENCES

1. Sakkalis, V., "Review of advanced techniques for the estimation of brain connectivity measured with eeg/meg," *Computers in Biology and Medicine*, Vol. 41, no. 12, pp. 1110–1117, 2011.

2. Lang, E. W., A. Tomé, I. R. Keck, J. Górriz-Sáez, and C. Puntonet, "Brain connectivity analysis: a short survey," *Computational Intelligence and Neuroscience*, Vol. 2012, p. 8, 2012.

3. Friston, K., "Causal modelling and brain connectivity in functional magnetic resonance imaging," *PLoS Biology*, Vol. 7, no. 2, p. 220, 2009.

4. Joel, S. E., B. S. Caffo, P. van Zijl, and J. J. Pekar, "On the relationship between seed-based and ica-based measures of functional connectivity," *Magnetic Resonance in Medicine*, Vol. 66, no. 3, pp. 644–657, 2011.

5. Lemieux, L., J. Daunizeau, and M. C. Walker, "Concepts of connectivity and human epileptic activity," *Frontiers in Systems Neuroscience*, Vol. 5, 2011.

6. Greenblatt, R., M. Pflieger, and A. Ossadtchi, "Connectivity measures applied to human brain electrophysiological data," *Journal of Neuroscience Methods*, Vol. 207, no. 1, pp. 1–16, 2012.

7. Sporns, O., "Brain connectivity," *Scholarpedia*, Vol. 2, no. 10, p. 4695, 2007. revision #91084.

8. Wager, T. D., and M. A. Lindquist, *Principles of fMRI*, Leanpub, 2015.

9. Richardson, M., "Current themes in neuroimaging of epilepsy: brain networks, dynamic phenomena, and clinical relevance," *Clinical Neurophysiology*, Vol. 121, no. 8, pp. 1153–1175, 2010.

10. Bénar, C.-G., C. Grova, E. Kobayashi, A. P. Bagshaw, Y. Aghakhani, F. Dubeau, and J. Gotman, "Eeg–fmri of epileptic spikes: concordance with eeg source localization and intracranial eeg," *NeuroImage*, Vol. 30, no. 4, pp. 1161–1170, 2006.

11. Fox, M. D., and M. E. Raichle, "Spontaneous fluctuations in brain activity observed with functional magnetic resonance imaging," *Nature Reviews Neuroscience*, Vol. 8, no. 9, pp. 700–711, 2007.

12. Lee, M. H., C. D. Smyser, and J. S. Shimony, "Resting-state fmri: a review of methods and clinical applications," *American Journal of Neuroradiology*, Vol. 34, no. 10, pp. 1866–1872, 2013.

13. Van Den Heuvel, M. P., and H. E. H. Pol, "Exploring the brain network: a review on resting-state fmri functional connectivity," *European Neuropsychopharmacology*, Vol. 20, no. 8, pp. 519–534, 2010.

14. Duru, A., and A. Ademoglu, "Epileptic source localization: Deep electrode measurements versus scalp eeg," *International Journal of Bioelectromagnetism*, Vol. 11, pp. 175–178, 2009.

15. Lantz, G., R. G. de Peralta, L. Spinelli, M. Seeck, and C. Michel, "Epileptic source localization with high density eeg: how many electrodes are needed?," *Clinical Neurophysiology*, Vol. 114, no. 1, pp. 63–69, 2003.

16. Husain, F. T., and S. A. Schmidt, "Using resting state functional connectivity to unravel networks of tinnitus," *Hearing Research*, Vol. 307, pp. 153–162, 2014.

17. Buckner, R. L., F. M. Krienen, and B. T. Yeo, "Opportunities and limitations of intrinsic functional connectivity mri," *Nature Neuroscience*, Vol. 16, no. 7, pp. 832–837, 2013.

18. Hampson, M., X. Shen, and R. T. Constable, "Functional connectivity mr imaging," in *Functional Neuroradiology*, pp. 355–371, Springer, Boston, MA, 2011.

19. Jensen, F. E., "Epilepsy in 2013: progress across the spectrum of epilepsy research," *Nature Reviews Neurology*, Vol. 10, no. 2, pp. 63–64, 2014.

20. Kandel, E. R., J. H. Schwartz, T. M. Jessell, *et al.*, "Seizures and epilepsy," in *Principles of Neural Science* (K., E., ed.), pp. 1116–1139, McGraw-Hill New York, 2013.

21. Lehnertz, K., G. Ansmann, S. Bialonski, H. Dickten, C. Geier, and S. Porz, "Evolving networks in the human epileptic brain," *Physica D: Nonlinear Phenomena*, Vol. 267, pp. 7–15, 2014.

22. Centeno, M., and D. W. Carmichael, "Network connectivity in epilepsy: resting state fmri and eeg–fmri contributions," *Frontiers in Neurology*, Vol. 5, p. 93, 2014.

23. Xiao, F., D. An, and D. Zhou, "Functional mri-based connectivity analysis: a promising tool for the investigation of the pathophysiology and comorbidity of epilepsy," *Seizure*, Vol. 44, pp. 37–41, 2017.

24. Liao, W., Z. Zhang, Z. Pan, D. Mantini, J. Ding, X. Duan, C. Luo, G. Lu, and H. Chen, "Altered functional connectivity and small-world in mesial temporal lobe epilepsy," *PloS One*, Vol. 5, no. 1, 2010.

25. Huang, H., and M. Ding, "Linking functional connectivity and structural connectivity quantitatively: a comparison of methods," *Brain Connectivity*, Vol. 6, no. 2, pp. 99–108, 2016.

26. Ryali, S., T. Chen, K. Supekar, and V. Menon, "Estimation of functional connectivity in fmri data using stability selection-based sparse partial correlation with elastic net penalty," *NeuroImage*, Vol. 59, no. 4, pp. 3852–3861, 2012.

27. Marrelec, G., A. Krainik, H. Duffau, M. Pélégrini-Issac, S. Lehéricy, J. Doyon, and H. Benali, "Partial correlation for functional brain interactivity investigation in functional mri," *NeuroImage*, Vol. 32, no. 1, pp. 228–237, 2006.

28. Chen, T., S. Ryali, S. Qin, and V. Menon, "Estimation of resting-state functional connectivity using random subspace based partial correlation: A novel method for reducing global artifacts," *NeuroImage*, Vol. 82, pp. 87–100, 2013.

29. Gökçay, D., "fmrg temel bilgiler," tech. rep., Middle East Technical University, 2007.

30. Bijsterbosch, J., S. M. Smith, and C. F. Beckmann, *An Introduction to Resting State fMRI Functional Connectivity*, Oxford University Press, 2017.

31. Biswal, B., F. Zerrin Yetkin, V. M. Haughton, and J. S. Hyde, "Functional connectivity in the motor cortex of resting human brain using echo-planar mri," *Magnetic Resonance in Medicine*, Vol. 34, no. 4, pp. 537–541, 1995.

32. Cole, D. M., S. M. Smith, and C. F. Beckmann, "Advances and pitfalls in the analysis and interpretation of resting-state fmri data," *Frontiers in Systems Neuroscience*, Vol. 4, 2010.

33. Mantini, D., M. G. Perrucci, C. Del Gratta, G. L. Romani, and M. Corbetta, "Electrophysiological signatures of resting state networks in the human brain," *Proceedings of the National Academy of Sciences*, Vol. 104, no. 32, pp. 13170–13175, 2007.

34. Cataldi, M., M. Avoli, and E. Villers-Sidani, "Resting state networks in temporal lobe epilepsy," *Epilepsia*, Vol. 54, no. 12, pp. 2048–2059, 2013.

35. Buckner, R. L., J. R. Andrews-Hanna, and D. L. Schacter, "The brain's default network," *Annals of the New York Academy of Sciences*, Vol. 1124, no. 1, pp. 1–38, 2008.

36. Fransson, P., and G. Marrelec, "The precuneus/posterior cingulate cortex plays a pivotal role in the default mode network: Evidence from a partial correlation network analysis," *NeuroImage*, Vol. 42, no. 3, pp. 1178–1184, 2008.

37. Stafstrom, C. E., and L. Carmant, "Seizures and epilepsy: an overview for neuroscientists," *Cold Spring Harbor Perspectives in Medicine*, Vol. 5, no. 6, p. a022426, 2015.

38. Wendling, F., P. Chauvel, A. Biraben, and F. Bartolomei, "From intracerebral eeg signals to brain connectivity: identification of epileptogenic networks in partial epilepsy," *Frontiers in Systems Neuroscience*, Vol. 4, p. 154, 2010.

39. Graan, L., L. Lemieux, and U. Chaudhary, "Scalp and intracranial eeg-fmri in epilepsy," *J Neurol Neurophysiol*, Vol. 4, no. 156, pp. 19–22, 2013.

40. Cárdenas-Rodríguez, N., L. Carmona-Aparicio, D. L. Pérez-Lozano, D. Ortega-Cuellar, S. Gómez-Manzo, and I. Ignacio-Mejía, "Genetic variations associated with pharmacoresistant epilepsy," *Molecular Medicine Reports*, Vol. 21, no. 4, pp. 1685–1701, 2020.

41. Haneef, Z., and D. K. Chen, "Functional neuro-imaging as a pre-surgical tool in epilepsy," *Annals of Indian Academy of Neurology*, Vol. 17, no. Suppl 1, p. S56, 2014.

42. O' Muircheartaigh, J., and M. P. Richardson, "Epilepsy and the frontal lobes," *Cortex*, Vol. 48, no. 2, pp. 144–155, 2012.

43. Vulliemoz, S., D. W. Carmichael, K. Rosenkranz, B. Diehl, R. Rodionov, M. C. Walker, A. W. McEvoy, and L. Lemieux, "Simultaneous intracranial eeg and fmri of interictal epileptic discharges in humans," *NeuroImage*, Vol. 54, no. 1, pp. 182–190, 2011.

44. Marino, A. C., G. J. Yang, E. Tyrtova, K. Wu, H. P. Zaveri, P. Farooque, D. D. Spencer, and S. K. Bandt, "Resting state connectivity in neocortical epilepsy: The epilepsy network as a patient-specific biomarker," *Clinical Neurophysiology*, Vol. 130, no. 2, pp. 280–288, 2019.

45. Zhang, J., W. Liu, H. Chen, H. Xia, Z. Zhou, L. Wang, S. Mei, Q. Liu, and Y. Li, "Eeg–fmri validation studies in comparison with iceeg: a review," *International Journal of Psychophysiology*, Vol. 84, no. 3, pp. 233–239, 2012.

46. Richardson, M. P., "Large scale brain models of epilepsy: dynamics meets connectomics," *Journal of Neurology, Neurosurgery & Psychiatry*, Vol. 83, no. 12, pp. 1238–1248, 2012.

47. Groening, K., V. Brodbeck, F. Moeller, S. Wolff, A. van Baalen, C. M. Michel, O. Jansen, R. Boor, G. Wiegand, U. Stephani, *et al.*, "Combination of eeg–fmri and eeg source analysis improves interpretation of spike-associated activation networks in paediatric pharmacoresistant focal epilepsies," *NeuroImage*, Vol. 46, no. 3, pp. 827–833, 2009.

48. Holt, A. B., and T. I. Netoff, "Computational modeling of epilepsy for an experimental neurologist," *Experimental Neurology*, Vol. 244, pp. 75–86, 2013.

49. Zhang, J., W. Liu, H. Chen, H. Xia, Z. Zhou, S. Mei, Q. Liu, and Y. Li, "Multimodal neuroimaging in presurgical evaluation of drug-resistant epilepsy," *NeuroImage: Clinical*, Vol. 4, pp. 35–44, 2014.

50. Amini, L., *Development of differential connectivity graph for characterization of brain regions involved in epilepsy.* PhD thesis, University of Grenoble, 2011.

51. Wurina, Y.-F. Z., and S.-G. Zhao, "Resting-state fmri studies in epilepsy," *Neurosci Bull*, Vol. 28, no. 4, pp. 449–455, 2012.

52. Lang, S., N. Duncan, and G. Northoff, "Resting-state functional magnetic resonance imaging: review of neurosurgical applications," *Neurosurgery*, Vol. 74, no. 5, pp. 453–465, 2014.

53. Haneef, Z., A. Lenartowicz, H. J. Yeh, J. Engel, and J. M. Stern, "Effect of lateralized temporal lobe epilepsy on the default mode network," *Epilepsy & Behavior*, Vol. 25, no. 3, pp. 350–357, 2012.

54. Tana, M. G., A. M. Bianchi, P. Vitali, F. Villani, and S. Cerutti, "Exploring interregional brain interactivity in temporal lobe epilepsy using partial correlation analysis of fmri data," in *30th Annual International Conference of the IEEE Engineering in Medicine and Biology Society*, pp. 4423–4426, IEEE, 2008.

55. Stoecklein, S., A. Hilgendorff, M. Li, K. Förster, A. W. Flemmer, F. Galiè, S. Wunderlich, D. Wang, S. Stein, H. Ehrhardt, *et al.*, "Variable functional connectivity architecture of the preterm human brain: Impact of developmental cortical expansion and maturation," *Proceedings of the National Academy of Sciences*, Vol. 117, no. 2, pp. 1201–1206, 2020.

56. Yeo, B. T., F. M. Krienen, J. Sepulcre, M. R. Sabuncu, D. Lashkari, M. Hollinshead, J. L. Roffman, J. W. Smoller, L. Zöllei, J. R. Polimeni, *et al.*, "The organization of the human cerebral cortex estimated by intrinsic functional connectivity," *Journal of Neurophysiology*, 2011.

57. Mueller, S., D. Wang, M. D. Fox, B. T. Yeo, J. Sepulcre, M. R. Sabuncu, R. Shafee, J. Lu, and H. Liu, "Individual variability in functional connectivity architecture of the human brain," *Neuron*, Vol. 77, no. 3, pp. 586–595, 2013.

58. Wang, H. E., C. G. Bénar, P. P. Quilichini, K. J. Friston, V. K. Jirsa, and C. Bernard, "A systematic framework for functional connectivity measures," *Frontiers in Neuroscience*, Vol. 8, 2014.

59. Sahin, D., "Functional connectivity network analysis of alzheimer and mild cognitive impairment patients," Master's thesis, Bogazici University, Istanbul, Turkey, 2014.

60. Jorge, J., W. Van Der Zwaag, and P. Figueiredo, "Eeg–fmri integration for the study of human brain function," *NeuroImage*, Vol. 102, pp. 24–34, 2014.

61. Calhoun, V. D., and T. Adali, "Unmixing fmri with independent component analysis," *IEEE Engineering in Medicine and Biology Magazine*, Vol. 25, no. 2, pp. 79–90, 2006.

62. McKeown, M. J., S. Makeig, G. G. Brown, T.-P. Jung, S. S. Kindermann, A. J. Bell, and T. J. Sejnowski, "Analysis of fmri data by blind separation into independent spatial components," *Human Brain Mapping*, Vol. 6, no. 3, pp. 160–188, 1998.

63. Hyvärinen, A., "Fast and robust fixed-point algorithms for independent component analysis," *IEEE transactions on Neural Networks*, Vol. 10, no. 3, pp. 626–634, 1999.

64. Norton, L., R. Hutchison, G. Young, D. Lee, M. Sharpe, and S. Mirsattari, "Disruptions of functional connectivity in the default mode network of comatose patients," *Neurology*, Vol. 78, no. 3, pp. 175–181, 2012.

65. Matthews, M., and D. A. Fair, "Research review: Functional brain connectivity and child psychopathology–overview and methodological considerations for investigators new to the field," *Journal of Child Psychology and Psychiatry*, Vol. 56, no. 4, pp. 400–414, 2015.

66. Cole, M. W., G. J. Yang, J. D. Murray, G. Repovš, and A. Anticevic, "Functional connectivity change as shared signal dynamics," *Journal of Neuroscience Methods*, Vol. 259, pp. 22–39, 2016.

67. Sanchez-Romero, R., and M. W. Cole, "Combining multiple functional connectivity methods to improve causal inferences," *Journal of Cognitive Neuroscience*, Vol. 33, no. 2, pp. 180–194, 2021.

68. Brier, M. R., A. Mitra, J. E. McCarthy, B. M. Ances, and A. Z. Snyder, "Partial covariance based functional connectivity computation using ledoit–wolf covariance regularization," *NeuroImage*, Vol. 121, pp. 29–38, 2015.

69. Hale, J. R., S. D. Mayhew, K. J. Mullinger, R. S. Wilson, T. N. Arvanitis, S. T. Francis, and A. P. Bagshaw, "Comparison of functional thalamic segmentation from seed-based analysis and ica," *NeuroImage*, Vol. 114, pp. 448–465, 2015.

70. van Oort, E., A. v. C. van Walsum, and D. G. Norris, "An investigation into the functional and structural connectivity of the default mode network," *NeuroImage*, Vol. 90, pp. 381–389, 2014.

71. Cribben, I., and Y. Yu, "Estimating whole-brain dynamics by using spectral clustering," *Journal of the Royal Statistical Society: Series C (Applied Statistics)*, Vol. 66, no. 3, pp. 607–627, 2017.

72. Ting, C.-M., A.-K. Seghouane, S.-H. Salleh, and A. Mohd Noor, "Estimation of high-dimensional brain connectivity from fmri data using factor modeling," in *2014 IEEE Workshop on Statistical Signal Processing (SSP)*, pp. 73–76, IEEE, 2014.

73. Hinne, M., R. J. Janssen, T. Heskes, and M. A. van Gerven, "Bayesian estimation of conditional independence graphs improves functional connectivity estimates," *PLoS Comput Biol*, Vol. 11, no. 11, p. e1004534, 2015.

74. Hoyle, D. C., "Accuracy of pseudo-inverse covariance learning-a random matrix theory analysis," *IEEE Transactions on Pattern Analysis and Machine Intelligence*, Vol. 33, no. 7, pp. 1470–1481, 2011.

75. Banerjee, O., L. E. Ghaoui, A. d'Aspremont, and G. Natsoulis, "Convex optimization techniques for fitting sparse gaussian graphical models," in *Proceedings of the 23rd international Conference on Machine Learning*, pp. 89–96, ACM, 2006.

76. Greve, D. N., and B. Fischl, "Accurate and robust brain image alignment using boundary-based registration," *NeuroImage*, Vol. 48, no. 1, pp. 63–72, 2009.

77. Barch, D. M., G. C. Burgess, M. P. Harms, S. E. Petersen, B. L. Schlaggar, M. Corbetta, M. F. Glasser, S. Curtiss, S. Dixit, C. Feldt, *et al.*, "Function in the human connectome: task-fmri and individual differences in behavior," *NeuroImage*, Vol. 80, pp. 169–189, 2013.

78. Baker, J. T., A. J. Holmes, G. A. Masters, B. T. Yeo, F. Krienen, R. L. Buckner, and D. Öngür, "Disruption of cortical association networks in schizophrenia and psychotic bipolar disorder," *JAMA Psychiatry*, Vol. 71, no. 2, pp. 109–118, 2014.

79. Benjamini, Y., and Y. Hochberg, "Controlling the false discovery rate: a practical and powerful approach to multiple testing," *Journal of the Royal Statistical Society: Series B (Methodological)*, Vol. 57, no. 1, pp. 289–300, 1995.

80. Shinn, A. K., J. T. Baker, K. E. Lewandowski, D. Öngür, and B. M. Cohen, "Aberrant cerebellar connectivity in motor and association networks in schizophrenia," *Frontiers in Human Neuroscience*, Vol. 9, p. 134, 2015.

81. Schmittmann, V. D., S. Jahfari, D. Borsboom, A. O. Savi, and L. J. Waldorp, "Making large-scale networks from fmri data," *PloS One*, Vol. 10, no. 9, p. e0129074, 2015.

82. Smith, S. M., K. L. Miller, G. Salimi-Khorshidi, M. Webster, C. F. Beckmann, T. E. Nichols, J. D. Ramsey, and M. W. Woolrich, "Network modelling methods for fmri," *NeuroImage*, Vol. 54, no. 2, pp. 875–891, 2011.

83. Schmidt, M., "L1precision: Matlab code for map estimation of gaussian graphical model precision with l1-regularizer.," 2006.

84. Xuan, X., and K. Murphy, "Modeling changing dependency structure in multivariate time series," in *Proceedings of the 24th International Conference on Machine Learning*, pp. 1055–1062, 2007.

85. Shcherbakov, M. V., A. Brebels, N. L. Shcherbakova, A. P. Tyukov, T. A. Janovsky, and V. A. Kamaev, "A survey of forecast error measures," *World Applied Sciences Journal*, Vol. 24, no. 24, pp. 171–176, 2013.

86. Junior, C. R. F., "Root mean square error (rmse)," tech. rep., Universidade Federal de Alagoas (UFAL).

87. Cornell, J., and R. Berger, "Factors that influence the value of the coefficient of determination in simple linear and nonlinear regression models," *Phytopathology*, Vol. 77, no. 1, pp. 63–70, 1987.

88. Zhang, Z., G. Lu, Y. Zhong, Q. Tan, W. Liao, Z. Chen, J. Shi, and Y. Liu, "Impaired perceptual networks in temporal lobe epilepsy revealed by resting fmri," *Journal of Neurology*, Vol. 256, no. 10, pp. 1705–1713, 2009.

89. Zhang, Z., G. Lu, Y. Zhong, Q. Tan, Z. Yang, W. Liao, Z. Chen, J. Shi, and Y. Liu, "Impaired attention network in temporal lobe epilepsy: a resting fmri study," *Neuroscience Letters*, Vol. 458, no. 3, pp. 97–101, 2009.

90. Su, L., J. An, Q. Ma, S. Qiu, and D. Hu, "Influence of resting-state network on lateralization of functional connectivity in mesial temporal lobe epilepsy," *American Journal of Neuroradiology*, Vol. 36, no. 8, pp. 1479–1487, 2015.

91. Shen, K., B. Mišić, B. N. Cipollini, G. Bezgin, M. Buschkuehl, R. M. Hutchison, S. M. Jaeggi, E. Kross, S. J. Peltier, S. Everling, *et al.*, "Stable long-range interhemispheric coordination is supported by direct anatomical projections," *Proceedings of the National Academy of Sciences*, Vol. 112, no. 20, pp. 6473–6478, 2015.

92. Spencer, S. S., "Neural networks in human epilepsy: evidence of and implications for treatment," *Epilepsia*, Vol. 43, no. 3, pp. 219–227, 2002.

93. Salzmann, A., and A. Malafosse, "Genetics of temporal lobe epilepsy: a review," *Epilepsy Research and Treatment*, Vol. 2012, 2012.

94. Stretton, J., G. Winston, M. Sidhu, M. Centeno, C. Vollmar, S. Bonelli, M. Symms, M. Koepp, J. S. Duncan, and P. J. Thompson, "Neural correlates of working memory in temporal lobe epilepsy–an fmri study," *NeuroImage*, Vol. 60, no. 3, pp. 1696–1703, 2012.

95. Pressl, C., P. Brandner, S. Schaffelhofer, K. Blackmon, P. Dugan, M. Holmes, T. Thesen, R. Kuzniecky, O. Devinsky, and W. A. Freiwald, "Resting state functional connectivity patterns associated with pharmacological treatment resistance in temporal lobe epilepsy," *Epilepsy Research*, Vol. 149, pp. 37–43, 2019.

96. Grassia, F., A. V. Poliakov, S. L. Poliachik, K. Casimo, S. D. Friedman, H. Shurtleff, C. Giussani, E. J. Novotny, J. G. Ojemann, and J. S. Hauptman, "Changes in resting-state connectivity in pediatric temporal lobe epilepsy," *Journal of Neurosurgery: Pediatrics*, Vol. 22, no. 3, pp. 270–275, 2018.

97. Buckner, R. L., "The brain's default network: origins and implications for the study of psychosis," *Dialogues in Clinical Neuroscience*, Vol. 15, no. 3, p. 351, 2013.

98. Zhang, C., H. Yang, W. Qin, C. Liu, Z. Qi, N. Chen, and K. Li, "Characteristics of resting-state functional connectivity in intractable unilateral temporal lobe epilepsy patients with impaired executive control function," *Frontiers in Human Neuroscience*, Vol. 11, p. 609, 2017.

99. de Campos, B. M., A. C. Coan, C. Lin Yasuda, R. F. Casseb, and F. Cendes, "Large-scale brain networks are distinctly affected in right and left mesial temporal lobe epilepsy," *Human Brain Mapping*, Vol. 37, no. 9, pp. 3137–3152, 2016.

100. Burianová, H., N. L. Faizo, M. Gray, J. Hocking, G. Galloway, and D. Reutens, "Altered functional connectivity in mesial temporal lobe epilepsy," *Epilepsy Research*, Vol. 137, pp. 45–52, 2017.

101. Brugger, S. P., and O. D. Howes, "Heterogeneity and homogeneity of regional brain structure in schizophrenia: a meta-analysis," *JAMA Psychiatry*, Vol. 74, no. 11, pp. 1104–1111, 2017.

102. Struck, A. F., and M. B. Westover, "Variability in clinical assessment of neuroimaging in temporal lobe epilepsy," *Seizure*, Vol. 30, pp. 132–135, 2015.

103. Pittau, F., C. Grova, F. Moeller, F. Dubeau, and J. Gotman, "Patterns of altered functional connectivity in mesial temporal lobe epilepsy," *Epilepsia*, Vol. 53, no. 6, pp. 1013–1023, 2012.

104. Rajpoot, K., A. Riaz, W. Majeed, and N. Rajpoot, "Functional connectivity alterations in epilepsy from resting-state functional mri," *PloS One*, Vol. 10, no. 8, p. e0134944, 2015.

105. Vincent, J. L., I. Kahn, A. Z. Snyder, M. E. Raichle, and R. L. Buckner, "Evidence for a frontoparietal control system revealed by intrinsic functional connectivity," *Journal of Neurophysiology*, Vol. 100, no. 6, pp. 3328–3342, 2008.

106. Scolari, M., K. N. Seidl-Rathkopf, and S. Kastner, "Functions of the human frontoparietal attention network: Evidence from neuroimaging," *Current Opinion in Behavioral Sciences*, Vol. 1, pp. 32–39, 2015.

107. Spreng, R. N., J. Sepulcre, G. R. Turner, W. D. Stevens, and D. L. Schacter, "Intrinsic architecture underlying the relations among the default, dorsal attention, and frontoparietal control networks of the human brain," *Journal of Cognitive Neuroscience*, Vol. 25, no. 1, pp. 74–86, 2013.

108. Cavanna, A. E., and M. R. Trimble, "The precuneus: a review of its functional anatomy and behavioural correlates," *Brain*, Vol. 129, no. 3, pp. 564–583, 2006.

109. Danielson, N. B., J. N. Guo, and H. Blumenfeld, "The default mode network and altered consciousness in epilepsy," *Behavioural Neurology*, Vol. 24, no. 1, pp. 55–65, 2011.

110. Haneef, Z., A. Lenartowicz, H. J. Yeh, H. S. Levin, J. Engel Jr, and J. M. Stern, "Functional connectivity of hippocampal networks in temporal lobe epilepsy," *Epilepsia*, Vol. 55, no. 1, pp. 137–145, 2014.

111. Corbetta, M., and G. L. Shulman, "Control of goal-directed and stimulus-driven attention in the brain," *Nature Reviews Neuroscience*, Vol. 3, no. 3, pp. 201–215, 2002.

112. Dumlu, S. N., "Investigation of semantic effects in oddball paradigm through event related potentials," Master's thesis, Middle East Technical University, Ankara, Turkey, 2012.

113. Basit, A., S. Ali Khan, W. Tariq Toor, N. Maroof, M. Saadi, and A. Ali Khan, "A novel dissimilarity of activity biomarker and functional connectivity analysis for the epilepsy diagnosis," *Symmetry*, Vol. 11, no. 8, p. 979, 2019.

114. Zalesky, A., A. Fornito, and E. Bullmore, "On the use of correlation as a measure of network connectivity," *NeuroImage*, Vol. 60, no. 4, pp. 2096–2106, 2012.

115. Bonilha, L., T. Nesland, G. U. Martz, J. E. Joseph, M. V. Spampinato, J. C. Edwards, and A. Tabesh, "Medial temporal lobe epilepsy is associated with neuronal fibre loss and paradoxical increase in structural connectivity of limbic structures," *Journal of Neurology, Neurosurgery & Psychiatry*, Vol. 83, no. 9, pp. 903–909, 2012.

116. DeSalvo, M. N., L. Douw, N. Tanaka, C. Reinsberger, and S. M. Stufflebeam, "Altered structural connectome in temporal lobe epilepsy," *Radiology*, Vol. 270, no. 3, pp. 842–848, 2014.